



The SKAO Pulsar Timing Array

Ryan M. Shannon,^{1,2} N. D. Ramesh Bhat,³ Aurélien Chalumeau,^{4,5} Siyuan Chen,^{6,18} H. Thankful Cromartie,⁷ A. Gopakumar,⁸ Kathrin Grunthal,⁹ Jeffrey S. Hazboun,¹⁰ Francesco Iraci,^{11,12} Bhal Chandra Joshi,^{13,14} Ryo Kato,¹⁵ Michael J. Keith,¹⁶ Kejia Lee,¹⁷ Kuo Liu,^{6,18} Hannah Middleton,¹⁹ Matthew T. Miles,^{20,2} Chiara M. F. Mingarelli,²¹ Aditya Parthasarathy,^{22,23,9} Daniel J. Reardon,^{1,2} Golam M. Shaifullah,^{24,25,12} Keitaro Takahashi,²⁶ Caterina Tiburzi,¹¹ Riccardo J. Truant,^{1,2} Xiao Xue,²⁷ Andrew Zic²⁸ and The SKA Pulsar Science Working Group

¹*Centre for Astrophysics and Supercomputing, Swinburne University of Technology, Hawthorn, VIC, 3122, Australia*

²*Australian Research Council Centre of Excellence for Gravitational Wave Astronomy (OzGrav)*

³*International Centre for Radio Astronomy Research, Curtin University, Bentley, WA 6102, Australia*

⁴*Laboratoire de Physique et Chimie de l'Environnement et de l'Espace, Université d'Orléans / CNRS, 45071 Orléans Cedex 02, France*

⁵*Observatoire Radioastronomique de Nançay, Observatoire de Paris, Université PSL, Université d'Orléans, CNRS, 18330 Nançay, France*

⁶*Shanghai Astronomical Observatory, Chinese Academy of Sciences, 80 Nandan Road, Shanghai 200030, P. R. China*

⁷*National Research Council Research Associate, National Academy of Sciences, Washington, DC 20001, USA resident at Naval Research Laboratory, Washington, DC 20375, USA*

⁸*Data Institute of Fundamental Research, II Homi Bhabha Road, Mumbai 400005, India*

⁹*Max-Planck-Institut für Radioastronomie, Auf dem Hügel 69, D-53121 Bonn, Germany*

¹⁰*Department of Physics, Oregon State University, Corvallis, OR 97331, USA*

¹¹*Dipartimento di Fisica, Università di Cagliari, Cittadella Universitaria, I-09042 Monserrato (CA), Italy*

¹²*INAF - Osservatorio Astronomico di Cagliari, via della Scienza 5, 09047 Selargius (CA), Italy*

¹³*National Centre for Radio Astrophysics, SP Pune University Campus, Pune 411007, Maharashtra, India*

¹⁴*Department of Physics, Indian Institute of Technology Roorkee, Roorkee 247667, Uttarakhand,*

¹⁵*Mizusawa VLBI Observatory, National Astronomical Observatory of Japan, 2-21-1 Osawa, Mitaka, Tokyo 181-8588, Japan*

¹⁶*Jodrell Bank Centre for Astrophysics, Department of Physics and Astronomy, University of Manchester, Manchester M13 9PL, UK*

¹⁷*Department of Astronomy, School of Physics, Peking University, Beijing 100871, P. R. China*

¹⁸*State Key Laboratory of Radio Astronomy and Technology, A20 Datun Road, Chaoyang District, Beijing, 100101, P. R. China*

¹⁹*Institute for Gravitational Wave Astronomy & School of Physics and Astronomy, University of Birmingham, Birmingham, United Kingdom*

²⁰*Department of Physics and Astronomy, Vanderbilt University, 2301 Vanderbilt Place, Nashville, TN 37235, USA*

²¹*Department of Physics, Yale University, New Haven, CT USA, 06520*

- ²²*ASTRON, Netherlands Institute for Radio Astronomy, Oude Hoogeveensedijk 4, 7991 PD Dwingeloo, The Netherlands*
- ²³*Anton Pannekoek Institute for Astronomy, University of Amsterdam, Science Park 904, 1098 XH Amsterdam, The Netherlands*
- ²⁴*Dipartimento di Fisica “G. Occhialini”, Università degli Studi di Milano-Bicocca, Piazza della Scienza 3, I-20126 Milano, Italy.*
- ²⁵*INFN, Sezione di Milano-Bicocca, Piazza della Scienza 3, 20126 Milano, Italy*
- ²⁶*Faculty of Advanced Science and Technology, Kumamoto University, Japan*
- ²⁷*Institut de Física d’Altes Energies (IFAE), The Barcelona Institute of Science and Technology, Campus UAB, 08193 Bellaterra (Barcelona), Spain*
- ²⁸*CSIRO, Space & Astronomy, Marsfield, NSW, 1710, Australia*

E-mail: rshannon@swin.edu.au

Pulsar timing arrays (PTAs) are ensembles of millisecond pulsars observed for years to decades. The primary goal of PTAs is to study gravitational-wave astronomy at nanohertz frequencies, with secondary goals of undertaking other fundamental tests of physics and astrophysics. Recently, compelling evidence has emerged in established PTA experiments for the presence of a gravitational-wave background. To accelerate a confident detection of such a signal and then study gravitational-wave emitting sources, it is necessary to observe a larger number of millisecond pulsars to greater timing precision. The SKAO telescopes, which will be a factor of three to four greater in sensitivity compared to any other southern hemisphere facility, are poised to make such an impact. In this chapter, we motivate an SKAO pulsar timing array (SKAO PTA) experiment. We discuss the classes of gravitational-wave sources present in PTA observations and how an SKAO PTA can detect and study them. We then describe the sources that can produce these signals. We discuss the astrophysical noise sources that must be mitigated to undertake the most sensitive searches. We then describe a realistic PTA experiment implemented with the SKA and place it in context alongside other PTA experiments likely ongoing in the 2030s. We describe the techniques necessary to search for gravitational waves in the SKAO PTA and motivate how very long baseline interferometry can improve the sensitivity of an SKAO PTA. The SKAO PTA will provide a view of the Universe complementary to those of the other large facilities of the 2030s.

1 Introduction

The last few decades have ushered in an era of multi-messenger astronomy: the study of the Universe through combining electromagnetic and non-electromagnetic signals (Hirata et al., 1987; Abbott et al., 2017b; IceCube Collaboration et al., 2018). One such non-electromagnetic signal is gravitational radiation: waves in the space-time metric. Like the electromagnetic spectrum, the gravitational-wave (GW) spectrum spans decades in frequencies.

GWs are produced by systems with large time varying mass quadrupole moments, which occur in systems like merging black holes or neutron stars. While the first indirect evidence for GWs came from the damping of the orbit of the Hulse-Taylor binary pulsar (Taylor and Weisberg, 1982; Hulse and Taylor, 1975), the first detection of GWs was by the LIGO (LIGO Scientific Collaboration et al., 2015) and Virgo (Acernese et al., 2015) Collaborations in 2015, with the ground-based laser interferometric detection of decahertz GWs from the inspiral of two $\sim 30 M_{\odot}$ black holes (Abbott et al., 2016). This was soon followed by the discovery of GWs from the merger of a binary neutron star system (Abbott et al., 2017b), for which electromagnetic radiation was also observed from a gamma-ray burst and kilonova associated with the merger (Abbott et al., 2017c), ushering in the era of multi-messenger GW astronomy. To date, the LIGO, Virgo and KAGRA (Akutsu et al., 2021) collaborations have made ~ 200 probable detections (LIGO Scientific Collaboration et al., 2025), with a fourth observation run ongoing. Ground-based laser interferometers are sensitive to GWs in the hertz to kilohertz regime, a band where signals originate from sources such as stellar mass black holes and neutron stars. While the observations directly proved Einstein’s prediction for the existence of GWs, they have also facilitated other breakthroughs across physics and astrophysics by providing a new way to observe the Universe with objects impossible to study otherwise (e.g., Abac et al., 2025).

Another band exists at much lower GW frequency that utilizes pulsars: rotating neutron stars that emit beams of radiation that span the electromagnetic spectrum. When the beams (misaligned with the rotation axis) cross our line of sight, we observe a pulse of radiation, which can be timed to exquisite precision. When observed in the radio band, the time-of-arrival of the pulses observed at Earth can be measured to precisions of better than hundreds of nanoseconds (Agazie et al., 2023a; Zic et al., 2023; EPTA Collaboration et al., 2023a; Chen et al., 2025; Miles et al., 2025a) for the most precise millisecond pulsars (MSPs): a subclass of rapidly rotating pulsars spun up due to accretion from a companion (Alpar et al., 1982; Backer et al., 1982).

It has long been known that GWs passing across the pulsar-Earth line of sight will alter the light propagation time from the pulsar to the Earth (Sazhin, 1978; Detweiler, 1979). Through the study of an ensemble of pulsars, called a pulsar timing array (PTA, Foster and Backer, 1990), it is possible to distinguish the presence of GW from other processes that alter pulse arrival times, as GWs impart distinctive angular correlations (Hellings and Downs, 1983) due to their quadrupolar nature, whereas other processes (often termed noise) are either uncorrelated between pulsars or show different spatial correlations (Tiburzi et al., 2016).

Pulsar timing observations are sensitive to GWs with frequencies between the reciprocals of the observation baseline (\sim years to decades) and twice the observing cadence (\sim days to months), which

is typically 1-100 nHz. In this band, the most likely source of GWs is binary supermassive black holes (SMBHs [Begelman et al., 1980](#)) in sub milliparsec orbits. After galaxies merge, the central SMBHs of the progenitors are dragged to the center of the merged system. Through dynamical and viscous friction, the black holes form a gravitationally bound system that continues to harden. When the black holes are sufficiently close, GW emission can dominate the inspiral. The superposition of GW from all supermassive black hole binaries (SMBHBs) in the Universe produces a stochastic GW background (GWB, [Hellings and Downs, 1983](#); [Rajagopal and Romani, 1995](#)). This is thought to be the first signal that a PTA experiment would detect ([Wyithe and Loeb, 2003](#)) The GWB induces red-noise or temporal correlations in pulse arrival times. This can be modeled as a power-law power spectrum with an amplitude and a known spectral index in the case of SMBHBs inspiralling due to GW emission alone ([Phinney, 2001](#)). A GWB could first emerge as red noise with statistically consistent properties, known as common noise ([Siemens et al., 2013](#)). However, the presence of Hellings-Downs angular correlations ([Hellings and Downs, 1983](#)) is necessary for a confident detection of the GWB ([Allen et al., 2023](#)), because it is possible to detect common noise in PTA data sets when no GWB is present ([Goncharov et al., 2021b](#); [Zic et al., 2022](#)). In addition to a GWB from the population of SMBHBs, other GW signals could exist in PTA data sets. This includes individual resolvable (spectrally and spatially) SMBHBs ([Sesana and Vecchio, 2010](#); [Agazie et al., 2025a](#)), bursts from SMBH flybys, and signals originating from exotic physical processes ([Wang et al., 2015](#); [Dandapat et al., 2023](#); [Afzal et al., 2023](#)). Detection and study of any of these signals not only confirm the presence of a fundamental component of the Universe, but also offers glimpses into regions otherwise invisible, either because the objects themselves are electromagnetically dim or embedded in centers of galaxies and obscured. Recent advances are summarized in [Mingarelli et al. \(2025\)](#).

PTA experiments have been ongoing for decades in Australia (The Parkes Pulsar Timing Array, PPTA, [Manchester et al., 2013](#); [Zic et al., 2023](#)), Europe (The European Pulsar Timing Array, EPTA, [Kramer and Champion, 2013](#); [EPTA Collaboration et al., 2023a](#)), and North America (The North American Nanohertz-frequency Gravitational Wave Observatory, NANOGrav, [Demorest et al., 2013](#); [Agazie et al., 2023a](#)). Observations have been taken with the most sensitive radio telescopes at metre-decimetre wavelengths, choosing this band as receivers are sensitive, pulsars are relatively bright, and the highest timing precision can in general be achieved. More recently PTA experiments have started in China (The Chinese Pulsar Timing Array, CPTA [Lee, 2016](#)), using the Five Hundred Metre Aperture Telescope (FAST); in India (The Indian Pulsar Timing Array, InPTA [Joshi et al., 2022](#)), using the upgraded Giant Metrewave Radio Telescope (uGMRT) and the Ootucmund Radio Telescope (ORT); and in South Africa (The MeerKAT Pulsar Timing Array, MPTA [Miles et al., 2023](#)), using the MeerKAT radio telescope. There is also now PTA analysis undertaken using observations of gamma-ray bright millisecond pulsars observed with the Fermi Space Telescope (The Gamma Ray Pulsar Timing Array, GPTA, [FERMI-LAT Collaboration et al., 2022](#)). The groups collaborate and share data as part of the International Pulsar Timing Array ([Hobbs et al., 2010](#); [Verbiest et al., 2016](#); [Perera et al., 2019](#)). More than 160 MSPs are observed as part of these efforts.

These projects have made great progress towards the definitive detection of nanohertz-frequency GWs through searching the data sets over the past decade. At the beginning of the 2020s, common

uncorrelated red noise was detected in NANOGrav (Arzoumanian et al., 2020a), EPTA (Chen et al., 2021), and PPTA (Goncharov et al., 2021b) data analyses. More recently, evidence has emerged for the presence of a GWB in PTA data sets (Agazie et al., 2023b; EPTA+InPTA Collaboration et al., 2023; Reardon et al., 2023b; Xu et al., 2023; Miles et al., 2025b). Hellings and Downs spatial correlations were identified in these searches with $\approx 2 - 4\sigma$ statistical significance; visualizations of these correlations can be found in Figure 1. While these analyses are consistent at the $1 - 2\sigma$ level (Agazie et al., 2024a), the amplitude of the signal is louder than found in some previous searches (Shannon et al., 2015; Reardon et al., 2023b). An increased sensitivity to GWs can be achieved by timing larger numbers of pulsars to higher precision (Siemens et al., 2013). This has been demonstrated through GW searches undertaken by the CPTA and MPTA, which have shown high sensitivity despite timing baselines more than a factor of three shorter than those of other PTA experiments.

With a significant increase in sensitivity relative to MeerKAT and the Murchison Widefield Array, and access to the same sky, the SKA Observatory (SKAO) telescopes (SKA-Low and SKA-Mid) promise to be important instruments for PTA science in the 2030s. There are two baseline deployments for the telescopes: AA* and AA4. The SKA-Low AA* deployment comprises 307 stations and AA4 comprises 512 stations. The SKA-Mid AA* deployment comprises 144 antennas, and AA4 comprises 197 antennas. Indeed, PTA GW searches have been long identified as a key project for the SKAO (Cordes et al., 2004). Here we update the previous PTA science case for the SKAO published nearly a decade ago (Janssen et al., 2015). We describe the types of GW signals that can be observed with the SKAO in Section 2. We then describe the sources that could emit these signals in Sections 3 and 4. In Section 5, we describe sources of contaminating noise in PTA data sets and how to best remove or mitigate them using the SKAO. In Section 6, we motivate a potential PTA programme for the SKAO, including requirements for observations, data products, and data analysis. We highlight the important roles that can be made by SKA Low telescope and very long baseline interferometry in Sections 8 and 7, respectively. In Section 9 we highlight the complementarity of high energy pulsar timing to the SKAO PTA. In Section 10 we outline some of requirements for the SKAO PTA. We connect the SKAO PTA to other science outcomes that will be achieved by the SKAO and other 2030s facilities in Section 11 and conclude the paper in Section 12.

2 Pulsar Timing Array Signals

There are a plethora of different source classes and signals that we might expect to detect with the SKAO PTA. We refer to objects or systems that produce gravitational waves as source classes. These sources can produce gravitational waves of different types (which we refer to as signals), which are searched for and studied using different techniques. Before we describe the sources of GWs we expect to observe, we describe the signals that can be measured, and motivate how the SKAO PTA has the potential to play a transformational role.

2.1 Gravitational-wave backgrounds

A GWB is the superposition of GWs from all of GW emitting sources. For an individual gravitational wave source, the strain h_{ij} at a distance d_L from a source with mass quadrupole moment Q_{ij} is

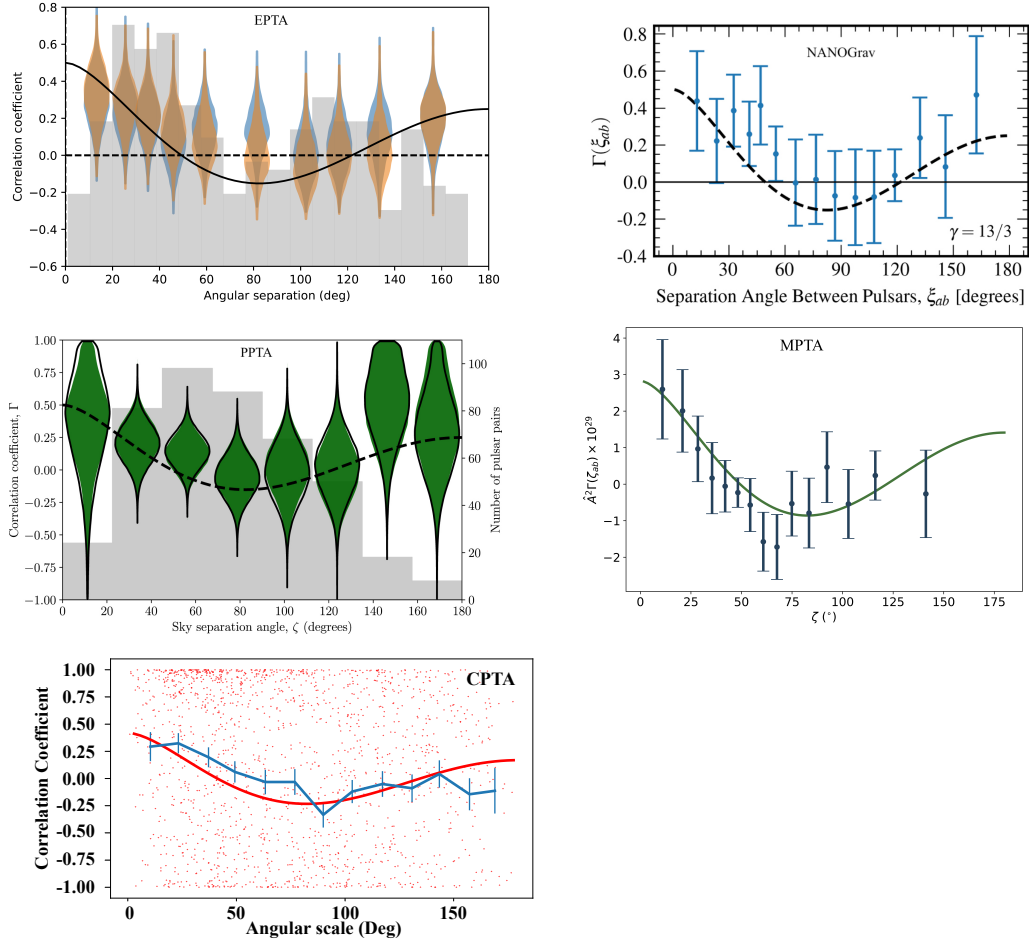


Figure 1: Inter-pulsar correlations from recent pulsar timing array gravitational-wave searches. We show the correlations derived from the the European Pulsar Timing Array and Indian Pulsar Timing Array (EPTA+InPTA Collaboration et al., 2023), the North American Nanohertz Observatory for Gravitational Waves (Agazie et al., 2023b), the MeerKAT Pulsar Timing Array (Miles et al., 2025b), the Parkes Pulsar Timing Array (Reardon et al., 2023b), and the Chinese Pulsar Timing Array (Xu et al., 2023).

(Abbott et al., 2017a)

$$h_{ij} = \frac{2}{c^4} \frac{G}{d_L} \frac{d^2}{dt^2} Q_{ij} \quad (1)$$

In the case of compact objects in a circular binary orbit, this can be approximated as (Peters and Mathews, 1963; Jaffe and Backer, 2003)

$$h = 4\sqrt{\frac{2}{5}} \left(\frac{G\mathcal{M}}{c^3}\right)^{5/3} \left(\frac{2\pi}{P_b}\right)^{2/3} \frac{c}{d_L} \quad (2)$$

$$\approx 1.2 \times 10^{-15} \left(\frac{\mathcal{M}}{10^9 M_\odot}\right)^{5/3} \left(\frac{P_b}{\text{yr}}\right)^{-2/3} \left(\frac{d_L}{\text{Gpc}}\right)^{-1} \quad (3)$$

where P_b is the binary orbital period, $\mathcal{M} = (m_1 m_2)^{3/5} / (m_1 + m_2)^{1/5}$ is the chirp mass, and m_1 and m_2 are the component masses. We note that sensitivity to GW strain scales $\propto d_L^{-1}$, unlike electromagnetic observations which scale $\propto d_L^{-2}$.

A GWB can be characterized by a strain spectrum, $h_c(f)$, which quantifies the gravitational wave strain amplitude emitted at different frequencies. The GWB is often assumed to follow a power law spectrum for astrophysically motivated reasons (e.g., [Phinney, 2001](#)). In this case, the strain spectrum is defined as

$$h_c(f) = A_{\text{yr}} \left(\frac{f}{f_{\text{yr}}} \right)^\alpha, \quad (4)$$

where A_{yr} is the characteristic amplitude of the GWB at a frequency of $f_{\text{yr}} = 1 \text{ yr}^{-1}$, and α is the strain spectral index. The most recent PTA analyses find $A_{\text{yr}} \approx 2 \times 10^{-15}$ ([Agazie et al., 2024a](#)).

The strain spectrum can be related to the closure energy density in GWs following

$$\Omega_{\text{gw}}(f) = \frac{2\pi^2}{3H_0^2} f^2 h_c^2(f), \quad (5)$$

where H_0 is the Hubble constant. For most expected backgrounds in the nanohertz-frequency band, the strain amplitude of GWs is expected to be greater at lower frequencies (i.e., $\alpha < 0$). For a GWB arising from SMBHBs, in circular orbits, hardening solely due to gravitational radiation, the exponent is expected to be $\alpha = -2/3$ ([Phinney, 2001](#)). Other sources, for example of cosmological origin, may produce a GWB with a different spectral index. This can be used to distinguish GWB from different sources.

To compare the GWB signal to other sources of noise in PTA data sets, the effect of the GWB is often expressed in terms of its power spectral density in the pulsar timing residuals, which is ([Siemens et al., 2013](#))

$$P_r(f) = \frac{A_{\text{yr}}^2}{12\pi^2} \left(\frac{f}{f_{\text{yr}}} \right)^{2\alpha-3}. \quad (6)$$

A GWB is manifested in two parts. The first part is a common red noise: time-correlated stochastic processes that are statistically independent in different pulsars but are drawn from the same underlying distribution. This is the combined effect of gravitational waves passing through the Earth and all of the pulsars. The second part has the same time-correlations as the common red noise, but is partially correlated between pulsars. This effect is related to the perturbations that GWs passing through the Earth induce on the times of arrival. The GWB induces angular correlations between pulsar pairs that follow the Hellings-Downs function ([Hellings and Downs, 1983](#)), which deviates from a pure quadrupole due to averaging over a large number of GW sources that are uniformly distributed across the sky with random GW polarization angles.

For PTAs with a small number of pulsars, the common red noise is expected to be the first signal detected. However, it is possible to mistakenly detect the presence of such a signal ([Goncharov et al., 2021b](#); [Zic et al., 2022](#)), due to the presence of other sources of noise (including pulsar spin noise, as discussed below). Thus, in order to confidently detect a GWB and study it robustly, it is necessary to also find the common correlations it induces across an ensemble of pulsars.

The sensitivity to a GWB can be improved through longer observing campaigns, observing with higher precision (or equivalently higher cadence), and observing a larger number of pulsars ([Siemens et al., 2013](#)). However, once a PTA is dominated by a common red noise with unclear correlations,

the improvement to sensitivity only scales weakly with the respect to the first two. Thus, the best way to improve the PTA sensitivity is to observe a larger sample of pulsars. With increased sensitivity and access to the southern sky, an SKAO PTA can include the largest sample of pulsars ever. With the ability to form multiple sub-arrays with the SKAO telescopes, the pulsars in the SKAO PTA can be observed efficiently.

2.2 Individual sources of gravitational waves

Continuous GW sources (CGWs) are the most considered individual sources of GWs (Agazie et al., 2023c; EPTA Collaboration et al., 2024b; Zhao et al., 2025). These are typically modeled as sinusoidal signals in pulsar timing residuals, as the sources thought to emit them (binary supermassive black holes, discussed below) are expected to be in circular orbits in the pulsar timing band, and can be decomposed into two parts: one representing the passage of the gravitational wave by the Earth (the Earth term) and the second passing the pulsar (the pulsar term). The amplitude of the signal depends on the GW strain and polarization, the relative positions of the source and the pulsar, and the pulsar distance. The distance of the pulsar is treated as an unknown if a pulsar distance is known to a precision greater than the GW wavelength (the case, currently, for most MSPs). GW searches also need to consider whether the source is evolving, in which case the frequency in the pulsar term might be different than that in the Earth term. While most searches consider these models, efforts are ongoing to model PTA responses to individual massive black holes spiraling along general relativistic eccentric orbits and understanding their implications for PTAs (Susobhanan et al., 2020; Susobhanan, 2023; Agazie et al., 2024b).

In addition to periodic sources, it is possible to search for transient GW bursts as well. Bursts with memory are semipermanent distortions in space-time caused by the merger of compact objects (Favata, 2010). They will manifest as sudden changes in the spin frequency of the pulsar. They could manifest as changes that are contemporaneous between pulsars and show the expected quadrupolar correlation (Pshirkov et al., 2010; van Haasteren and Levin, 2010). Alternatively, pulsar term memory bursts would manifest in an individual pulsar (Cordes and Jenet, 2012). Bursts produced by other sources may have different wave forms. Hyperbolic passages of SMBHBs in general relativistic hyperbolic orbits could provide bursts with linear memory sources in the PTA frequency window (Dandapat et al., 2023, 2024).

2.3 Beyond backgrounds: gravitational wave maps

If the nanohertz GWB is primarily generated by SMBHBs in massive galaxies, its angular anisotropies should mirror the cosmic large-scale structure (LSS) (Semenzato et al., 2024) at low GW frequencies, or be dominated by loud individual binaries at high frequencies (Mingarelli et al., 2013). Otherwise, a GWB can also originate from a wide range of early-Universe processes, such as red-shifted primordial GWs (Lasky et al., 2016; Domènech, 2021), phase transitions (Caprini et al., 2020; Hindmarsh et al., 2021) or cosmic string collapse (Hiramatsu et al., 2014), discussed further below. The majority of these cosmological models predict an isotropic GWB.

Hence, a pillar stone of identifying the origin of the GWB is searching for variations in GW across the sky. Most commonly, the GW power is expanded in spherical harmonics (Mingarelli et al.,

2013), where the corresponding coefficients are determined from the PTA data. The resulting sky distribution is visualized in terms of sky maps, the so-called anisotropy maps.

Recent simulation-based studies coupling halo catalogs, semi-analytic SMBHB population models, and PTA map-making pipelines demonstrate that cross-correlations between GWB anisotropy maps and galaxy clustering can recover this imprint at high significance once PTAs achieve multipole sensitivities of $\ell_{\max} \gtrsim 40\text{--}70$. In this regime, loud nearby binaries behave as Poisson-like contaminants, and become visible as stand-out hot-spots on the sky map that can be modeled or excised, allowing the residual anisotropy to act as a novel cosmological tracer (Semenzato et al., 2024). The local angular resolution of a PTA data set is intimately linked to the number of pulsars it comprises, and their sky distribution (Boyle and Pen, 2012; Ali-Haïmoud et al., 2020, 2021; Grunthal et al., 2026).

The broad sky coverage and timing precision of the SKAO PTA will be decisive in realizing this measurement, enabling anisotropy maps of sufficient resolution to probe the spatial distribution of SMBHB hosts and, ultimately, to connect the nanohertz GWB to the cosmic web itself (Semenzato et al., 2024).

2.4 Ultra-low frequency gravitational waves

The SKA timing era also opens a complementary pHz window ($10^{-16}\text{--}10^{-9}$ Hz) by exploiting slow, GW-induced drifts in pulsar timing parameters rather than residuals. A Bayesian analysis of pulsar orbital period derivatives \dot{P}_b and spin second derivatives \ddot{P} across many millisecond pulsars sets competitive limits today and forecasts SKAO-enabled sensitivity to continuous pHz signals from early-stage SMBHBs (and some cosmological scenarios) (Zheng et al., 2026). It may also be possible to search for low frequency gravitational waves through the study of binary pulsar orbital frequency derivatives, which are also affected by GWs (Kopeikin, 1997). This approach bridges the gap between cosmic microwave background and PTA frequencies, leverages long baselines without overfitting away ultra-low-frequency content, and adds orthogonal evidence to residual-based searches like PTAs. With improved timing precision of SKAO PTA and new pulsar discoveries, parameter-drift searches become a realistic avenue for first pHz-band detections (Zheng et al., 2026).

3 Gravitational waves from supermassive black hole binaries

We now summarize how supermassive black hole binaries manifest in the pulsar timing band and the astrophysics that can be gleaned through their observation.

3.1 Gravitational-wave backgrounds

SMBHs are expected to reside at the center of all massive galaxies (Kormendy and Ho, 2013). As two galaxies merge, the two central SMBHs will come closer to each other and eventually form a gravitationally bound binary (Thorne and Braginskii, 1976). The evolution of the binary is driven by several mechanisms: dynamical friction, stellar hardening, and interactions with gaseous disks are the main contributors. The question of which mechanism is the dominant one that drives the binary to shrink down to sub-pc scale has been termed the final parsec problem (Milosavljević and

Merritt, 2003). Eventually, when the distance is below \sim pc, the binary will merge as the orbital energy diminishes through the emission of GWs (Begelman et al., 1980). This hierarchical process produces SMBHBs of increasingly greater masses (Volonteri et al., 2003). As the SMBHBs slowly spiral into each other they emit GWs related to their orbital period (see equation 2). These GWs can be measured by PTAs and are thus a major candidate for the possible source of the PTA signal.

The energy emitted in GWs depends on the properties of the SMBHBs and the physics driving the evolution. For an individual binary, this manifests in the frequencies at which GWs are emitted. For a circular SMBHB purely driven by GW emission the GW frequency is twice the orbital frequency. Eccentric binaries and environmental evolution will cause deviation from the power law. The most prominent effect is a shallower spectrum at low frequencies, corresponding to long orbital periods, as this is where environmental evolution dominates over the GW emission (Ravi et al., 2014; Kelley et al., 2017).

Assuming that the GWB is composed of signals from circular SMBHBs, the resulting characteristic strain follows a power-law described by Eq. (4) with slope $\alpha = -2/3$ and amplitude A determined by the underlying population model (Phinney, 2001). If one takes into account the environmental effect and non-zero eccentricity, the characteristic strain manifests a broken power-law pattern with a spectral turnover, which could occur at frequencies near $\sim 3 \times 10^{-9}$ Hz. A single broken power-law model can be modeled as (Sampson et al., 2015; Arzoumanian et al., 2020a):

$$h_c(f) = A_{\text{yr}} \left(\frac{f}{\text{yr}^{-1}} \right)^\alpha \left[1 + \left(\frac{f}{f_{\text{break}}} \right)^{1/\ell} \right]^{\ell(\beta - \alpha)}, \quad (7)$$

where f_{break} is the transition frequency, ℓ affects the smoothness of the transition and β is the spectral index describing the power law at high frequencies compared to α at lower frequencies. The phenomenological model can then be compared against astrophysically motivated models to determine the driving mechanism of the SMBHB evolution. The SKAO PTA will initially contribute by measuring the properties of a GWB at high frequency, with lower frequency properties inferred from the combination of SKAO PTA and legacy IPTA data sets.

Finally, a finite-number-of-sources effect challenges the Gaussian ensemble assumption, which would also cause a spectral turn-over at frequencies $> 10^{-8}$ Hz (Sesana et al., 2008; Agazie et al., 2025a). This effect can also be accounted for by introducing a model based prior distribution for $h_c(f)$ (Agazie et al., 2025a). With the SKAO PTA, we may be able to measure this effect and use it to infer the properties of the population.

3.2 Continuous gravitational-wave signals from individual supermassive black hole binaries

The SKAO PTA will also enable exquisite study of individual supermassive black hole binaries. With SKAO-enabled PTAs, it will become possible to probe the relativistic dynamics of SMBHBs in a regime inaccessible to any other experiment. Eccentric binaries or binaries whose frequency evolution are influenced by environmental effects, will emit GWs at multiple frequencies with different powers (Kocsis and Sesana, 2011; Sesana, 2013; Ravi et al., 2014; Chen et al., 2017). If measured by PTAs, this can be a hint as to the exact mechanism driving the evolution of

the SMBHB. For bright CGW sources where both the Earth and pulsar terms can be coherently recovered, the $\sim 10^3$ yr phase separation between these signals encodes post-Newtonian corrections to the orbital evolution, including measurable signatures of the binary mass ratio and spin-orbit coupling (Mingarelli et al., 2012). The timing precision and parallax-based distance determinations (discussed further below), enhanced by joint Gaia and pulsar-timing analyses (Moran et al., 2023), make recovery of the pulsar term feasible for a subset of high-mass, higher-frequency systems, allowing direct inference of component masses and spin parameters. This capability transforms PTA detections from statistical evidence of a GWB into precision probes of weak-field general relativity and the astrophysical evolution of massive binaries over millennia (Mingarelli et al., 2012).

It is also possible to use electromagnetic observations to enhance the sensitivity to sources of individual GWs. Targeted searches benefit by having fewer trial factors as positions and binary periods can be well constrained and can increase Bayes factors by a few to ten (Liu and Vigeland, 2021; Agarwal et al., 2025; Cardinal Tremblay et al., 2026). Non detections constrain supermassive black hole binary masses. Optical periodicity catalogs provide sky position, frequency priors, and luminosity distances that boost PTA sensitivity to individual binaries (Agarwal et al., 2025). This turns the SKAO PTA into an active experiment directly hunting for supermassive black hole binaries in their host galaxies, linking radio pulsar timing with optical variability, possible VLBI imaging of hosts, and future IR spectroscopy to test the binary hypothesis for binary candidates, source by source (Arzoumanian et al., 2020b; Xin et al., 2021; Agarwal et al., 2025; Casey-Clyde et al., 2025). Forecasts for the detection of individual sources can also be made through the use of cosmological simulations, indicating that SMBHBs will be detectable at SKAO sensitivities (Kelley et al., 2018). These prospects are investigated in further detail in Section 6.2.

These considerations open up the exciting prospect of pursuing persistent, multi-messenger nanohertz GW astronomy with promising inspiraling supermassive black-hole binaries (Joshi et al., 2022; Mingarelli et al., 2025). The evidence for the presence of nHz GW emitting SMBHBs in blazars OJ 287 and PKS 2131–021, possible because of decades-long multi-wavelength EM observations, adds real substance to this possibility (Dey et al., 2018; Laine et al., 2020; Traianou et al., 2025; Kiehlmann et al., 2025).

At the sensitivities and redshift reach of the SKAO PTA, strong gravitational lensing will become an important factor in the detection and interpretation of CGWs. Lensing magnification of $\mu \sim 2$ –100 can raise intrinsically faint binaries above the SKAO detection threshold, substantially increasing the number of resolvable systems and extending the PTA horizon to $z \gtrsim 2$ (Khusid et al., 2023). The same phenomenon can produce multiple gravitationally lensed images with measurable time delays, offering an unprecedented opportunity to test the coherence of GW and electromagnetic signals across cosmological distances. Because lensed hosts trace overdense environments, lensing will also modulate the angular distribution of individually resolvable binaries, a feature that the expanded sky coverage and pulsar yield of SKAO will uniquely allow us to characterize. In this way, the SKAO PTA will open a new window onto the population of supermassive black hole binaries in the high-redshift Universe (Khusid et al., 2023).

4 Gravitational-wave and related signals from the early universe

In addition to GWs from supermassive black holes, an SKAO PTA has the possibility to detect GWs predicted by fundamental physical processes. Several early-Universe processes—quantum fluctuations during inflation, first-order phase transitions (FOPTs), and topological defects—could have generated GWs (Allen, 1996; Caprini and Figueroa, 2018). Their spectra are characterized by $\Omega_{\text{gw}}(f)$, directly linked to the observable strain $h_c(f)$ (Planck Collaboration et al., 2020) as shown in Equation 5.

4.1 Cosmic inflation

Inflation explains the observed flatness and isotropy while predicting nearly scale-invariant perturbations (Grishchuk, 1974; Guth, 1981; Linde, 1982; Starobinsky, 1979). Quantum fluctuations produce scalar and tensor modes, the latter forming a stochastic GWB (Grishchuk, 1977). The tensor-to-scalar ratio $r < 0.036$ (95% C.L.) (Campeti and Komatsu, 2022; Tristram et al., 2022) constrains the amplitude, while the spectral index $n_t = 4/(1 + 3w) + 2$ is linked to the effective equation of state w . Slow-roll models ($w > -1$) give red-tilted spectra ($n_t < 0$) that fall steeply at PTA frequencies; stiff or phantom phases ($w < -1$) can yield blue tilts enhancing nanohertz power (Kuroyanagi et al., 2015; Lasky et al., 2016; Cai et al., 2021; Ferreira et al., 2024). The inflationary GWB (Zhao et al., 2013)

$$\Omega_{\text{gw}}^{\text{IGW}}(f) \simeq 1.1 r \times 10^{10n_t - 15} \left(\frac{f}{\text{yr}^{-1}} \right)^{n_t}, \quad (8)$$

implies $\Omega_{\text{gw}} < 10^{-16}$ for $r \sim 10^{-2}$, $n_t \sim -0.01$, though blue or stiff reheating scenarios may reach $\sim 10^{-10}$ – 10^{-9} (Liu et al., 2023).

Scalar-induced GWs arise from large curvature perturbations generating second-order tensor modes during radiation domination (Ananda et al., 2007; Baumann et al., 2007; Saito and Yokoyama, 2009). For curvature power $P_{\mathcal{R}}(k)$, the induced GWB is

$$\Omega_{\text{gw}}^{\text{SIGW}}(f) \propto \int du dv \mathcal{K}(u, v) P_{\mathcal{R}}(uk) P_{\mathcal{R}}(vk) \quad (9)$$

(Espinosa et al., 2018; Kohri and Terada, 2018), and peaks at $f \sim 10^{-9}$ – 10^{-8} Hz for $A_\zeta \sim 10^{-2}$ at $k \sim 10^{6-7} \text{ Mpc}^{-1}$ (Afzal et al., 2023; EPTA Collaboration et al., 2024a).

4.2 First-order phase transitions

Strong FOPTs driven by vacuum bubble nucleation can produce GWs through collisions, sound waves, and turbulence (Witten, 1984; Hogan, 1986; Kamionkowski et al., 1994; Caprini et al., 2009; Schwaller, 2015; Caprini and Figueroa, 2018; Guo et al., 2021). The dominant sound-wave term (Hindmarsh et al., 2014)

$$\Omega_{\text{gw}}^{\text{sw}} \propto v_w \left(\frac{H_*}{\beta} \right) \left(\frac{\kappa \alpha_*}{1 + \alpha_*} \right)^2 S(f/f_{\text{sw}}), \quad (10)$$

depends on bubble speed v_w , transition strength α_* , and inverse duration β/H_* . The peak frequency $f_{\text{sw}} \simeq 2 \times 10^{-5} \text{ Hz} (\beta/H_*) (T_*/100 \text{ GeV})/v_w$ shows that $T_* \sim 100$ – 300 MeV transitions fall in the PTA range (Xue et al., 2021; Afzal et al., 2023; EPTA Collaboration et al., 2024a; Athron et al., 2024). A smaller turbulent component scales as $(\epsilon_{\text{turb}} \alpha_*)^{3/2}$ with $\epsilon_{\text{turb}} \lesssim 0.05$ (Caprini et al., 2009).

4.3 Topological defects

In Beyond Standard Model particle physics, the early Universe may undergo symmetry breaking as it cools down, leaving relic defects whose dynamics radiate GWs. Discrete breaking forms *domain walls* decaying as the Universe expands (Vilenkin, 1981; Hiramatsu et al., 2014), producing

$$\Omega_{\text{gw}}^{\text{dw}} \propto \tilde{\epsilon} \left(\frac{\alpha_*}{0.01} \right)^2 S(f/f_{\text{dw}}), \quad f_{\text{dw}} \sim 10^{-9} \text{Hz} \left(\frac{T_*}{10 \text{MeV}} \right), \quad (11)$$

with efficiency $\tilde{\epsilon}$, energy fraction α_* , and annihilation temperature T_* (Ferreira et al., 2023). Their spectra at higher frequencies are flatter than FOPT signals. *Cosmic strings*, 1D defects from $U(1)$ breaking, form loops radiating via oscillation and cusps (Kibble, 1976; Vachaspati and Vilenkin, 1985; Allen and Shellard, 1992), yielding

$$\Omega_{\text{gw}}^{\text{cs}} \sim \sum_k (G\mu)^2 P_k \mathcal{I}_k(f), \quad (12)$$

where $G\mu$ is string tension and $P_k \propto k^{-q}$ ($q \sim 1$) (Lorenz et al., 2010; Gouttenoire et al., 2020). PTAs now probe $G\mu \sim 10^{-11}$ – 10^{-8} (Yonemaru et al., 2021; Quelquejay Leclere et al., 2023; Afzal et al., 2023).

4.4 Non-GW and exotic correlated signals

PTAs also respond to coherent non-GW phenomena that mimic or add to the GWB. This includes signals caused by dark matter. Some models predict dark matter is produced by low mass particles, which can interact with normal matter through gravitation, and potentially through scalar or vector fields.

Ultralight dark matter (ULDM) with $m \lesssim 10^{-18}$ eV produces coherent oscillations (Khmelnitsky and Rubakov, 2014; Porayko and Postnov, 2014; Porayko et al., 2018; Xia et al., 2023; Wu et al., 2022; Hu et al., 2026), yielding a common signal $|\delta t| \simeq 0.02 \text{ ns} (m/10^{-22} \text{eV})^{-2} (\rho_{\text{DM}}/0.4 \text{ GeV cm}^{-3})$ at $f_0 \simeq 4.8 \times 10^{-8} \text{ Hz} (m/10^{-22} \text{eV})$. PTA analyses exclude gravitational ULDM down to $m \lesssim 10^{-21}$ eV and place competitive limits on conformal couplings (Smarra et al., 2023, 2024; EPTA Collaboration et al., 2024a; Afzal et al., 2023).

If a dark matter scalar field couples to photons via a Chern–Simons term (Chern and Simons, 1974), it rotates the linear polarization of pulsar emission, i.e., cosmic birefringence (Sikivie, 1983; Carroll et al., 1990). The induced angle difference $\Delta\theta(t) = g[a(t - r_{\text{psr}}/c, \mathbf{x}_{\text{psr}}) - a(t, 0)]$ depends on coupling g and field a , producing correlated sky patterns (Liu et al., 2020; Caputo et al., 2019; Castillo et al., 2022; Liu et al., 2023; Li et al., 2025). Polarimetry limits from EPTA DR2 and the PPTA DR3 have been used to set complementary bounds on axion-like dark matter (Porayko et al., 2025; Xue et al., 2026).

Vector fields kinetically mixing with photons or gravitons can produce narrow-band strain backgrounds with $\Omega_{\text{gw}} \sim 10^{-13}$ – 10^{-11} near $f \sim 10^{-8}$ – 10^{-6} Hz (Co et al., 2022). If vector fields couple with Standard Model particles, their effect can be directly observed in PTA (Xue et al., 2022). Scalar–tensor couplings to baryonic mass or α variations induce time-dependent potentials (Arvanitaki et al., 2015; Blas et al., 2017); PTA data constrain $g_\phi \lesssim 10^{-9}$ for $m_\phi \sim 10^{-23}$ – 10^{-21} eV (Nomura et al., 2020). PTA observations are also capable of detecting dark matter substructures (Siegel et al., 2007; Lee et al., 2021; Kim and Mitridate, 2024) through gravitational effects.

4.5 Other early-Universe contributions

Additional mechanisms may add subdominant low-frequency power: An “Audible axion” is an axion or axion-like particle that couples with dark photons (Machado et al., 2019; Ellis et al., 2024); primordial gravitational collapses can also introduce a signal (Zeng et al., 2025); relic-neutrino damping altering the tensor slope (Weinberg, 2004; Boyle and Steinhardt, 2008); and modulated reheating or curvature variations imprinting secondary tensor modes (Domènech, 2021; Inomata et al., 2021).

PTAs thus probe physics from QCD and dark-sector transitions to axion-like and vector dark matter, providing a direct window onto pre-recombination dynamics. The SKA Observatory will be able to contribute by accurately measuring the properties of the signals it detects. The large number of pulsars and high timing precision will enable the spatial and temporal correlations of all signals measured to be precisely characterized.

5 Noise sources in pulsar timing array experiments

In order to study the sources of nanohertz frequency GWs and make best use of a PTA, it is essential to identify, model, and, where possible, eliminate noise from the observations.

In addition to thermal noise innate to a telescope (which can be reduced through lower system temperature and mitigated with larger gain, longer integration times, and wider bandwidths), pulsar timing observations include additional sources of noise that are largely astrophysical in origin (Cordes and Shannon, 2010; Verbiest and Shaifullah, 2018; Agazie et al., 2023d).

The noise processes are usually divided into phenomenological classes, based on their degree of temporal correlation and chromaticity, i.e., the dependence on radio frequency. Processes (assumed to be) uncorrelated between individual observing epochs are termed “white noise” sources. Red noise processes exhibit long time correlations between observations. They are often characterized in the Fourier domain by a red power-law spectrum. We note that the terms red and white do not imply the degree of chromaticity.

Noise processes can be achromatic, affecting all frequencies of radio emission identically. A GWB comprises one such red noise source. However, many processes show a high degree of chromaticity (Cordes and Shannon, 2010; Shannon and Cordes, 2017), and these are often among the strongest sources of noise in MSP observations. While many noise sources are expected to be spatially uncorrelated, there are stochastic processes associated with an observatory, the Earth, and the Solar system that can be common to all pulsars (Tiburzi et al. (2016)). The nature of the noise, and the covariance of the noise with GW signals of interest, dictate how it is best mitigated.

5.1 Red noise sources

5.1.1 Spin noise

It is well known that slowly spinning canonical pulsars exhibit rotational irregularities that manifest as spin noise (Groth, 1975). While millisecond pulsars are much more stable rotators, they are also intrinsically unstable at some level (Shannon and Cordes, 2010). The noise can potentially induce

fluctuations in residuals with similar redness to that of a GWB, potentially causing false detections of a common noise (Zic et al., 2022). It has also been proposed to use population level models for spin noise (Goncharov et al., 2022; van Haasteren, 2024) to derive unbiased properties of the GWB. Such models could be developed using MSP observations observed as part of the SKAO-PTA and the IPTA, in combination with studies of spin noise in young (non-recycled) pulsar timing data sets.

5.1.2 Secular profile variability

Pulsar timing typically assumes that the observed profile converges to an identical pulse profile at each epoch when calculating pulse times of arrival (TOAs). If this assumption is broken there will be biases in measured pulse arrival times. While secular changes in pulse shape have been known about non-recycled pulsars for half a century (Backer, 1970), only recently have shape variations been observed in millisecond pulsars. The most dramatic event was the sudden and significant distortion in the pulse profile of (at the time) one of the most important millisecond pulsars for PTA work, PSR J1713+0747 (Singha et al., 2021; Jennings et al., 2024; Mandow et al., 2025). However, it has also been observed in other millisecond pulsars (Liu et al., 2015; Shannon et al., 2016; Goncharov et al., 2021a), and is relatively prevalent in slower spinning pulsars (Lower et al., 2025). Some MSPs also show evidence for mode changing (Miles et al., 2022; Nathan et al., 2023), in which the pulse profile appears to converge to one of two (or a few) distinct states (Backer, 1970).

GWs do not cause pulse shape variability. Pulse timing techniques that both simultaneously model pulse shape variability and search for signal of interest can break covariances between shape variations and GWs in timing measurements. Such techniques have been developed (Lentati et al., 2017; Miles et al., 2022; Nathan et al., 2023; Larsen et al., 2024) and will become important with the high fidelity pulse profiles SKAO PTA will deliver.

5.2 Noise from the interstellar medium

As radio waves propagate through the interstellar medium (ISM), they are affected by the tenuous ionized interstellar medium (IISM). The medium disperses the radio emission due to a frequency-dependent refractive index, resulting in radio emission at lower frequencies arriving later than that at higher frequencies. The degree of refraction and hence dispersion depends on the density of the interstellar medium, with the dispersion dependent on the total column density, which is measured in units of dispersion measure (DM, see Tiburzi et al. 2026).

As the pulsar, Earth, and IISM move, the pulsar-Earth line of sight probes different columns of plasma. The largest stochastic process in the arrival times arises from variations in dispersion measure (You et al., 2007; Lam et al., 2016b; Donner et al., 2020).

As the IISM is inhomogeneous (Armstrong et al., 1995), the variable refractive index affects the propagation direction of the radio emission. This results in multi-path propagation effects, where radio waves travelling along many lines of sight are received at the telescope. The effects can be bifurcated into diffractive and refractive effects which cover the results of propagation effects on small and larger scales respectively. In pulsar timing observations diffractive effects manifest as diffractive scintillation and pulse broadening (Rickett, 1990). This multi-path propagation produces frequency-dependent timing delays that typically scale close to ν^{-4} to $\nu^{-4.4}$. Those

stochastic scattering variations introduce additional chromatic noise in the timing data, which typically modeled assuming a power law. Crucially, scattering noise is distinguishable from DM noise through wide-band observations. Recent PTA works have identified significant scattering noise in multiple pulsars (Reardon et al., 2023a; EPTA Collaboration et al., 2023b; Singha et al., 2024). The wider frequency coverage and enhanced sensitivity of SKAO telescopes will render scattering noise increasingly prominent, necessitating careful modeling of scattering noise.

To mitigate propagation effects, it is necessary to observe pulsars at a range of radio frequencies. For PTA experiments aiming at GW detection, timing precision at ‘infinite frequency’ – i.e., the timing precision after correcting the dispersion measure fluctuations – is crucial. Optimal observing strategies have been studied (Lee et al., 2012; Lam et al., 2018; Iraci et al., 2024; Kulkarni et al., 2025), and both the waveform driven (NANOGrav Collaboration et al., 2015) and the stochastic model-driven method (Lee et al., 2014) to correct dispersion measure fluctuations have been developed. Concurrent observations spanning wide ranges of radio frequency, particularly using multiple sub-arrays and radio frequencies between 30 MHz to 2 GHz, have shown the potential to measure DM variations up to sixth decimal places, significantly mitigating chromatic noise associated with DM variations, scattering and solar wind (Donner et al., 2020; Joshi et al., 2022; Tarafdar et al., 2022; Rana et al., 2025; Susarla et al., 2024). The SKAO telescopes provide this wide frequency coverage, with SKA-Mid telescope’s band 1, 2 and 5, together with SKA-Low telescope providing nearly continuous frequency coverage from 50 MHz to 15 GHz. Such wide frequency coverage and high sensitivity at frequencies above 3 GHz provide a unique opportunity to decouple the achromatic and chromatic noise processes from e.g. dispersion measure and scattering variations (Donner et al., 2020; Joshi et al., 2022; Lee et al., 2012). This will be especially important in the SKAO era, where more distant pulsars (which are more strongly affected by propagation effects) will be included in PTAs.

5.3 White noise sources

5.3.1 Jitter Noise

Pulsar radio emission exhibits clear pulse-to-pulse variability, a phenomenon long observed in canonical pulsars. In recent years, this variability has also been revealed in a number of MSPs (e.g., Osłowski et al., 2014; Liu et al., 2015, 2016; Parthasarathy et al., 2021; Liu et al., 2022; Gitika et al., 2025), thanks to the construction of highly sensitive telescopes and the development of high-time-resolution data recording systems. The variation can be either systematic, such as sub-pulse drifting and mode change (e.g., Weltevrede et al., 2006; Liu et al., 2016; Miles et al., 2022), or stochastic. The stochastic process introduces random phase and amplitude variations in integrated pulse profiles, and thus in their arrival time measurements, which can exceed the level expected from radiometer noise. This process, termed jitter noise (Cordes and Shannon, 2010; Liu et al., 2012) is present in all pulsar observations but dominates when the signal-to-noise ratio of individual pulses exceeds unity. In this regime the pulse shape variations are expected to be larger than the radiometer noise (Cordes and Shannon, 2010). In the case of MSPs, this is the case for the brightest pulsars, or with sensitive telescopes such as the SKAO (Liu et al., 2011; Shannon et al., 2014).

On narrow frequency scales, the jitter noise is fully correlated across the band and of the same amplitude (e.g., Liu et al., 2012). However, it is likely that jitter noise is not fully broad band and de-correlates over fractional bandwidths close to unity (e.g., Shannon et al., 2014; Kulkarni et al., 2024). The magnitude of jitter noise also depends on observing frequency. Several studies have reported that the magnitude of jitter noise in millisecond pulsars such as PSR J0437–4715 tends to increase toward lower frequencies (Shannon et al., 2014; Parthasarathy et al., 2021). However, recent InPTA measurements of PSR J0437–4715 with the uGMRT have provided jitter amplitudes in the low-frequency range (300 – 500 MHz), finding values comparable to those at higher frequencies around 1.4 GHz. This result may challenge previous studies which suggested that jitter amplitude increases at lower frequencies, and implies that low-frequency observations in future SKAO surveys may not always be severely limited by jitter noise (Kikunaga et al., 2024). These studies further demonstrate that for timing analysis using wide-band data, jitter noise may need to be modeled independently in multiple parts of the band (e.g., Goncharov et al., 2021a; Reardon et al., 2023a; Kulkarni et al., 2024).

Jitter noise is expected to decrease as the square-root of the number of pulses averaged, and thus integration time as well. In addition, some frameworks have been developed to mitigate jitter noise from the outset. This can be accomplished using either integrated pulse profiles (e.g., Osłowski et al., 2011), or directly single pulses (Kerr, 2015; Nathan et al., 2023). So far, none of the schemes has been successfully implemented in a long-term PTA dataset. The SKAO sensitivity will enable detailed study of single pulses for a large number of PTA MSPs, providing the best opportunity to facilitate jitter noise mitigation in the PTA timing dataset.

The flexibility of SKAO telescopes also allows for a more efficient observing strategy, when strong jitter noise is present. For bright pulsars limited by jitter noise, SKAO telescopes can be divided into sub arrays (Joshi et al., 2022; Gitika et al., 2025), where individual sub-arrays are observing different pulsars. This effectively provides more observing time, significantly aiding the jitter-dominated situation (Lee et al., 2012). In analysis of MSPs observed as part of the MPTA, Gitika et al. (2025) found that for 10 of the 83 pulsars, more than half of the observations were jitter dominated. However this increased to over half of the sample when extrapolating to SKAO sensitivity, assuming the AA4 configuration.

5.3.2 Other white noise sources

There are several other types of white-noise sources that can be present in a PTA dataset (Liu et al., 2011). For instance, stochastic variations in the pulse broadening can also introduce short term variations in the pulse profile. The stochasticity arises from stochasticity in the scatter broadened image of the pulsar and is termed the finite-scintle effect (Cordes and Shannon, 2010). Instrument-related effects caused by radio frequency interference, imperfect polarization calibration, insufficient bit sampling can also distort the shape of integrated profiles and introduce systematic bias in their arrival times. Additionally, errors in the cross-correlation to measure the arrival times can also introduce white noise in the timing data (Liu et al., 2011). This can be caused by significant mis-match of the template shape to the intrinsic pulsar signal.

5.4 Spatially correlated noise sources

It is of utmost importance to mitigate the effects of processes that can impart signals that are correlated between pulsars. [Tiburzi et al. \(2016\)](#) investigated many of the noise sources that can introduce such spatial correlations. The most common spatial correlations are monopolar and dipolar correlations, which reflect processes related to the spacetime reference frame. Pulsar timing is necessarily undertaken in an inertial reference frame ([Lorimer and Kramer, 2004](#)). The arrival time measurements are referred to local atomic clocks, which need to be transferred to TT(BIPM), the most stable terrestrial time (TT) standard. The arrival time at the observatory should also be transferred to the solar system barycentre, using a solar system ephemeris (SSE) which provides the positions of the major objects in the solar system (e.g., DE440, [Park et al., 2021](#)). Errors in the terrestrial time standard affect all pulsars in the same way and would induce a monopolar correlation. In contrast, errors in the solar system ephemeris would induce a dipolar correlation.

Such spatial correlations are noise processes in the context of GW detection, but serve as important means to construct a pulsar-based spacetime reference frame. The long-term stability of some MSPs is comparable to that of an atomic clock, so it is potentially possible to improve the performance of terrestrial time scales using PTA data ([Hobbs et al., 2012, 2020](#)). PTA observations can be used to measure the mass of major planets and massive asteroids in the solar system and constrain possible unmodeled objects in the solar system ([Champion et al., 2010](#); [Caballero et al., 2018](#); [Guo et al., 2018](#)). Despite the precision achievable using current timing data, the special meaning of the pulsar timing method is to provide a completely independent way to examine the space-time standard.

In terms of GW searches, such spatially correlated noise needs to be carefully checked and mitigated or modeled. PTAs provide a good way to check the transfer from the observatory time standard to TT. If the time transfer is performed correctly, the error in TT(BIPM) is less concerning for the current timing precision. Errors in solar system ephemeris were thought to be an important source of noise budgets for PTA data, and SSE errors may induce measurable biases on the GW detection statistics obtained from PTA data sets ([Arzoumanian et al., 2018](#)). However, the more recent searches have been found to be insensitive to the choice of SSE ([Arzoumanian et al., 2020a](#); [Goncharov et al., 2021b](#); [Chen et al., 2021](#)). The covariance between SSE errors and the GWB signal could depend on the specifics of the data set, such as the timing precision, the total time span, and the number of pulsars. For SKAO PTA with high timing precision and (initially) short data span, the role of SSE error still needs to be examined.

Several approaches have been developed to model the SSE uncertainties. One way relies on the fact that an SSE error has dipolar correlation, such as searching for dipolar-correlated red noise ([Tiburzi et al., 2016](#)), or using spherical harmonics to subtract the dipolar mode ([Roebber, 2019](#)). Another approach is to directly correct the timing residuals based on the physical model of the solar system, including a mass-perturbation method ([Champion et al., 2010](#)), quasi-Keplerian approximation ([Vallisneri et al., 2020](#)), or numerical dynamical model ([Guo et al., 2019, 2024](#)).

5.5 The solar wind

The solar wind (SW) introduces time-variable dispersion delays in pulsar signals that must be modeled as part of the PTA noise budget. The SW plasma is a medium that the line-of-sight of all

of the PTA pulsars cross – therefore, if not correctly mitigated, it induces spatial correlations that can mimic a false GWB detection (Tiburzi et al., 2016). Until 2022, PTA analyses corrected for a simple $1/r^2$ SW model (with r being the distance from the Sun) using a constant electron density at 1 AU, as implemented in standard pulsar timing software (Edwards et al., 2006; Madison et al., 2019). However, static models are insufficient: residual DM fluctuations of $\sim 10^{-4}$ – 10^{-3} pc cm⁻³ remain (Tiburzi et al., 2019), especially near solar conjunctions, and can bias other noise and timing parameters or mimic low-frequency signals (Lam et al., 2016a; Madison et al., 2019; Liu et al., 2025). The dynamic state of the SW and its detectability in pulsar-based measurements has been known for decades (Counselman and Rankin, 1972; Bird et al., 1980), but only recently have PTA analyses begun integrating these effects rigorously into the noise model.

Recently, linear Gaussian process (GP) models have been developed (Hazboun et al., 2022b; Nițu et al., 2024; Susarla et al., 2024) that treat the SW amplitude as a time-variable stochastic process, enabling the electron density at 1 AU to vary smoothly in time. This approach improves over the standard static correction and has been implemented in PTA pipelines such as *enterprise* (Ellis et al., 2020). The current PTA approach to SW modeling was presented in Susarla et al. (2024), where the authors finalized the “SW GP” algorithm developed in Hazboun et al. (2022b) and tested it over a decade of LOFAR data. The authors also demonstrated strong correlations between SW variability and average SW electron density, and pulsar ecliptic latitude. In particular, this confirms the trend presented in Tiburzi et al. (2021) with high-latitude pulsars showing SW-induced DM trends following the Solar cycle over years, and where low-latitude pulsars displaying instead elevated and more stochastic DM progresses, consistent with the slow solar wind.

Such data-driven modeling enables the separation of heliospheric and interstellar dispersion and improves timing precision near solar conjunction. Transient events—such as coronal mass ejections (CMEs)—require separate detection (Shaifullah et al., 2020) and treatment. Krishnakumar et al. (2021) reported a CME-induced DM spike in PSR J2145–0750, and similar use of pulsars for CME detection has been demonstrated by Wood et al. (2020).

6 A realistic pulsar timing array for the SKA Observatory

The most recent PTA searches have data sets that had spans of 3 – 25 years and ended in years ranging from 2020 (Agazie et al., 2023b; EPTA Collaboration et al., 2023a) to 2023 (Miles et al., 2025a). With the commencement of observations with AA*, an additional 7 – 10 years of data will likely be acquired and many ongoing PTA experiments will have achieved > 25 yr of observation by then. The increased timing baselines, complemented by the larger number of pulsars being observed will presumably have resulted in a $> 5\sigma$ detection of a GWB by then, based on domain defined criteria (Allen et al., 2023). This motivates the development of a pulsar timing experiment capable of prosecuting post GWB detection science, and one that complements and makes use of the legacy of the IPTA data sets (Verbiest et al., 2016; Perera et al., 2019).

Here we provide a forecast for what one type of PTA observing campaign with the SKAO telescopes could look like, to highlight the key role SKAO can play in future PTA experiments. We emphasize that this campaign is not fully optimized. We expect full optimization of the SKAO PTA to be

developed over the coming years. We focus our efforts on precision timing with SKA-Mid, and consider both the AA* and AA4 deployments. We can base our forecast on observations of a census of MSPs (Spiewak et al., 2022) undertaken with MeerKAT as part of the MeerTime Large Survey project (Bailes et al., 2020). 189 recycled pulsars visible to the SKA-Mid telescope were observed at more than 8 epochs using the MeerKAT L-band observing system. A smaller subset of > 80 have been observed more regularly as part of the MeerTime PTA (Miles et al., 2023, 2025a).

A formalism for calculating PTA sensitivity to both backgrounds and individual sources has been developed (Hazboun et al., 2019), extending on previous sensitivity forecasting methodologies (Siemens et al., 2013). The formalism can be used both to estimate the signal to noise ratio of a GWB (of specified amplitude and spectral index) or individual source (of specified amplitude and emitting frequency). It can also be used to generate sensitivity curves commonly used to characterize GW detectors.

The strategy outlined here is further motivated by understanding the sensitivity of a PTA depends on fundamental properties of the timing campaign: the number of pulsars observed (N_{psr}) the observing cadence c , timing precision σ_{WN} , and total observing span T . Rosado et al. (2015) and Lam (2018) show that the scaling relationships for the detection of single sources do not differ markedly from those for the stochastic background. In the weak signal regime, Siemens et al. (2013) calculated that the signal to noise ratio scales proportional to

$$S/N \propto N_{\text{psr}} \frac{c}{\sigma_{\text{WN}}^2} T^\beta, \quad (13)$$

where the timing precision and cadence are assumed to be the same for all pulsars in the array. In the low signal to noise ratio regime, the sensitivity increases strongly with both number of pulsars and observing span. In the strong signal regime, Siemens et al. (2013) calculated that the signal to noise ratio scales proportional to

$$S/N \propto N_{\text{psr}} \left(\frac{c}{\sigma^2} \right)^{1/2\beta} T^{1/2}. \quad (14)$$

In the strong signal regime, while sensitivity still scales strongly with number of pulsars, sensitivity only slowly changes with time $\propto T^{1/2}$, as the GWs act as self noise. The transition between weak and strong signal regimes occurs at $\approx N_{\text{psr}}$ (Rosado et al., 2015). This further motivates observing the largest sample of pulsars. While the scaling relationships are the same for the GWB and individual sources, realistic populations of binary supermassive black holes imply sensitivity at higher GW frequency could improve detection prospects, which entail modest changes to observing strategy (within a fixed total observing time, Baier et al., 2025).

We assume that AA* is a factor of three more sensitive than MeerKAT and that AA4 is a factor of four more sensitive than MeerKAT. For SKA-mid AA4 is forecast¹ to have a system equivalent flux density (SEFD) of 1.7 Jy and AA* is expected to have a SEFD of 2.4 Jy in band 2, compared to the 6 – 7 Jy SEFD for MeerKAT. SKA mid band 2 and MeerKAT L-band cover similar frequency ranges, with the former sensitive from 950 – 1760 MHz and the latter from 856 – 1712 MHz. We do

¹https://www.skao.int/sites/default/files/documents/SKAO-TEL-0000818-V2_SKA1_Science_Performance.pdf

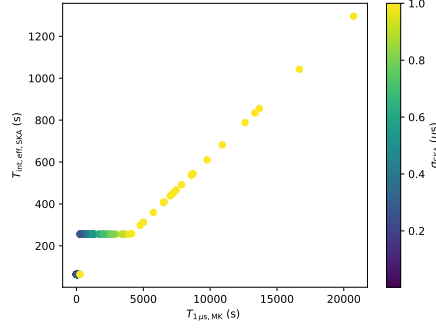


Figure 2: *Effective integration time for a SKAO-PTA. Pulsars for which the effective integration time is 64 μ s are observed in a MeerKAT-size sub-array for 256 s. The points are shaded by the timing precision achieved by the SKA observations.*

not expect to see any appreciable difference in timing precision from the telescope backends as both are designed using similar principles (including coherent dedispersion). We thus base estimates of arrival time precisions obtained from the MeerTime MSP census (Spiewak et al., 2022) and the MPTA (Miles et al., 2023). We can use spectral index measurements from the MSP census to extrapolate achievable timing precision to different observing bands.

We base our strategy on what has been implemented with the MPTA. We calculate the amount of time it takes to achieve 1 μ s timing precision for a pulsar using either SKAO or a MeerKAT sized sub-array. It is observed with a MeerKAT-size subarray if such timing precision can be achieved in < 256 s. If a pulsar can be observed with 1 μ s timing precision with AA* or AA4 in less than 256 s, then it is observed for that duration. For pulsars that require > 256 s to achieve this timing precision we observe for that duration. Pulsars that require ≥ 2000 s of integration time are not considered for inclusion in the array. We assume an observing cadence of two weeks.

We find that such an array can observe 174 MSPs with 8.9 hr of integration time with AA4. For AA* the array can achieve similar timing precision with 12.4 hr integration time per epoch. Under this strategy, 52 pulsars are observed in a MeerKAT-sensitivity sub-array for 256 s (effective array usage time of 64 s, 100 pulsars are with full SKA-sensitivity for 256 s and the remainder for up to 1300 s. The use of sub-arrays saves 2.8 hours per epoch, assuming all pulsars would be observed for at least 256 s with the full array. This highlights the importance of sub-arrays in enhancing observing efficiency. A comparison of the integration time of the pulsars in the array, to the time to achieve 1 μ s precision with MeerKAT can be found in Figure 2. Further array optimisation will be developed in advance of SKA deployment. A similar strategy, chosen for use by the MPTA without the use of sub-arrays, can achieve the same goals with 12 hr integration time per epoch on 83 MSPs.

6.1 Sensitivity to a GWB

Forecasts for PTA sensitivity to a GWB based on scaling relations of Siemens et al. (2013) can be seen in Figure 3. We compare the forecast sensitivity of this proposed SKAO timing program with ongoing PTA experiments as they were operational in 2020, assuming a GWB of amplitude

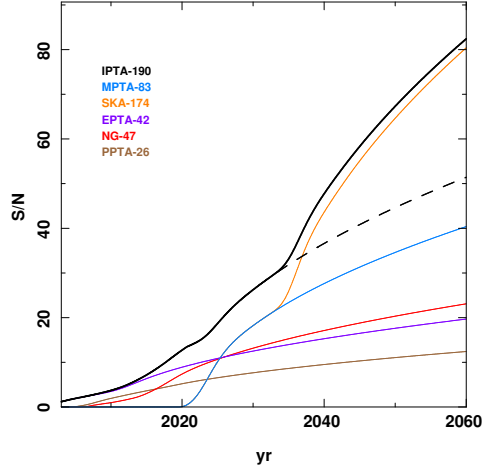


Figure 3: Comparison of PTA sensitivities. For the EPTA, MPTA, NANOGrav, and IPTA the curves are calculated assuming the observing strategies of the early 2020s. The number next to the name of the PTA in the legend indicates the number of pulsars observed by the PTA at that time. The IPTA curve is calculated by including all pulsars timed as part of PTA experiments. The solid black curve shows the projected sensitivity of the IPTA including the SKAO-PTA; the dashed black curve in the absence of the SKAO-PTA. The curves were calculated using methodology discussed in (Spiewak et al., 2022).

of $A_{\text{yr}} = 2 \times 10^{-15}$. The sensitivity uses the median timing precision and cadence observed for each pulsar as part of a given timing array. When an array has a smaller number of pulsars, signal to noise ratio soon scales with time $\propto T^{1/2}$ (where T is the observing span), as the GWB becomes self noise for itself, as discussed above. With a large number of pulsars timed to high precision, the SKAO-PTA dominates the international sensitivity within four years of operation. The SKAO-PTA continues to increase in sensitivity quickly as the array remains in the intermediate signal limit for longer owing to the larger number of pulsar pairs (Rosado et al., 2015), as discussed above. This highlights the importance of the inclusion of faint pulsars in a PTA that may require longer integration times.

Array sensitivity can be also visualized and assessed through sensitivity curves. These curves show array sensitivity to either a GWB or sky averaged sensitivity to an individual source. In Figure 4, we show sensitivity curves for the SKAO PTA after 5, 10, and 20 years of observing, and compare them to that from the MPTA 4.5 year data release (Miles et al., 2025a) and NANOGrav 15-year data set (Agazie et al., 2023a). We find that compared to other PTA experiments that the SKAO-PTA will have greater sensitivity across the GW spectrum. These sensitivity curves can also be used to forecast a signal to noise ratio. We find results that are in general agreement with those calculated using scaling relations as presented above.

We emphasize that the sensitivity calculations presented above are likely to be significantly refined considering the wide range of frequencies available to SKAO. In a strategy similar to that employed by InPTA using the SKA pathfinder telescope uGMRT, concurrent observations using different sub-arrays observing with Band 1 and 2 at the SKA-Mid telescope simultaneously with the SKA-Low telescope will provide more accurate instantaneous DM, scatter broadening, and solar wind

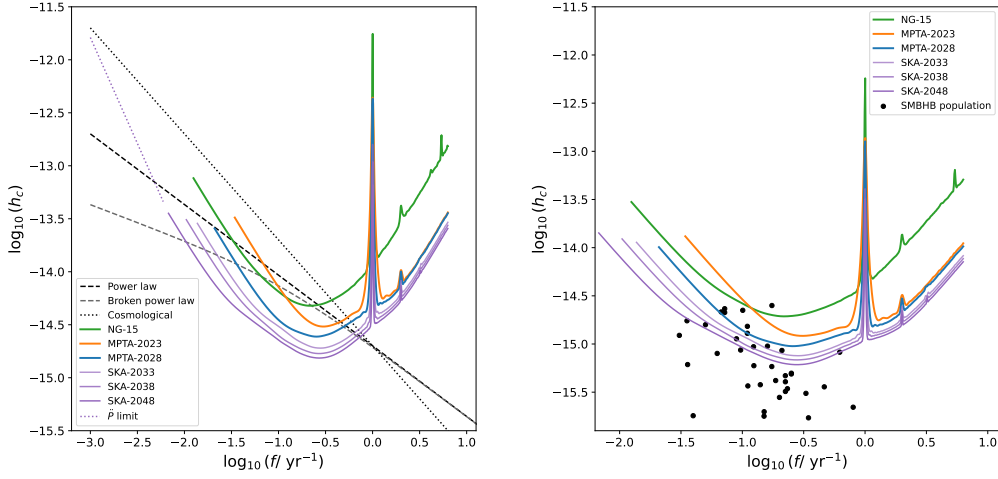


Figure 4: Strain sensitivity curves for the MeerKAT Pulsar Timing Array and a conceptual SKAO Pulsar Timing Array after observing for 5, 10, and 15 years. The left panel shows the sensitivity to a GWB. The black dashed lines shows the spectrum of a SMBHB driven GWB at an amplitude of $A_{\text{yr}} = 2 \times 10^{-15}$ for a power law (top) and broken power law (lower) as specified in Equation 7. The black dash dotted line shows the spectrum from a $A_{\text{yr}} = 2 \times 10^{-15}$ driven by inflation. The magenta dash dotted lines shows the expected sensitivity to ultra-low frequency gravitational waves using measurements of pulsar spin period second derivative (\dot{P}). The right panel shows the sky-averaged sensitivity to single source. The black points highlight individual sources detectable by the PTA. The curves highlight where pulsar timing array experiments have the greatest sensitivity.

measurements. Currently, the near simultaneous measurements by most PTAs implies that such characterization of chromatic noise is limited by the day-to-day fluctuations in the IISM biasing both the white and red noise posteriors. The resultant reduction in the sensitivity can therefore be avoided by adopting such observing strategy. The two telescope nature of SKAO, the wide primary beam of the SKA-Low telescope, the flexibility of using multiple sub-arrays with 16 pulsar timing beams in both the SKA-Low and SKA-Mid telescopes allow such flexible, efficient and more effective observing strategies (See Joshi et al., 2022, for possible configurations of the two SKAO telescopes that can be used).

Furthermore, additional MSPs suitable for inclusion in an SKAO PTA have been found since the MeerTime MSP census was undertaken (e.g., Clark et al., 2023; Kerr et al., 2025), and will continue to be discovered into the SKA era (Keane et al., 2026). This will allow for further expansion and optimization of the SKAO PTA.

6.2 Prospects for detecting individual sources

To assess the detectability of individual continuous gravitational wave (CGW) sources, we use the signal-to-noise (S/N) computation introduced in (Truant et al., 2025), applied to a 200 SMBHB populations generated with the L-Galaxies semi-analytical model (Izquierdo-Villalba et al., 2022), applied on the Millennium simulation (Springel et al., 2005). We consider the same SKAO PTA observing strategy used to search for and study a GWB described in the previous sections, in particular, an array comprising 174 known pulsars.

The total noise power spectral density of each pulsar is given by

$$S_k(f) = S_w + S_{\text{GW}}(f), \quad (15)$$

where $S_w = 2\Delta t_{\text{cad}}\sigma_w^2$ quantifies the stochastic uncertainty in pulse arrival times, Δt_{cad} is the cadence time, which will be typically two weeks. σ_w encodes all the temporal uncorrelated noise processes related to the telescope sensitivity and pulse instability (see Section 5.3). The term $S_{\text{GW}}(f)$ represents the GWB noise power spectral density, produced by an inspiralling SMBHB population, evaluated at a given frequency bin of the array (i.e., $\Delta f_i = [i/T_{\text{obs}}, (i+1)/T_{\text{obs}}]$, with $i = 1, \dots, N$).

As such, the strain-squared (h_c^2) associated with each frequency bin can be written as

$$h_c^2(f_i) = \sum_{j=1}^{N_S} \sum_{n=1}^{\infty} h_{c,n,j}^2(nf_k) \delta(\Delta f_i - nf_k), \quad (16)$$

where the sum is over all sources, N_S , and $\delta(\Delta f_i - nf_k)$ is a delta function that selects only SMBHBs emitting within the considered frequency bin. The index n accounts for the GW emission of eccentric binaries, which is distributed across harmonics of the orbital frequency. $h_{c,n,j}^2(f)$ is the squared characteristic strain of the source j . The value of $h_{c,n}^2$ is given by [Amaro-Seoane et al. \(2010\)](#).

We compute the S/N, and a CGW emitted by an SMBHB is considered resolved if its S/N exceeds 3. Once resolved, its contribution is subtracted from the SGWB; consequently, the noise budget in the pulsar array is reduced. This lower noise enhances the detectability of fainter CGWs. We repeat this process, reassessing the detectability of the remaining sources with the updated GWB, until no further sources are resolvable. In Figure 5, we show the median number of resolvable sources as a function of the observing time. The result, though idealized, highlights the capability of the SKAO PTA to resolve multiple CGW in the following years.

The pulsars sky position and location of resolved CGW for a single SMBHB population are shown in Figure 6.

6.3 Merit of the SKAO PTA for GW sky maps

The SKAO PTA can not only improve over current PTAs in terms of the sensitivity, but also in terms of the sky resolution. The long-term timing with the SKAO telescopes will significantly improve the accuracy of the pulsar distance, enabling the arc-min level resolution of the GW sky ([Lee et al., 2011](#)). In the short run, due to the limited pulsar distance precision, GW strain at the pulsar can not be coherently modeled. As demonstrated in [Grunthal et al. \(2026\)](#), decreasing the angular scale of the GWB fluctuations that a PTA can resolve is a key ingredient to increasing the detectability of small angular scale deviations from isotropy, such as caused by a single, stand-out SMBHB. There are of course challenges. For example, [Semenzato et al. \(2025\)](#) showed that truncating the angular power distribution at any ℓ_{max} causes power from the higher order multipoles to leak down into the lower order ones, inducing a bias. This will also need to be resolved when interpreting maps of the GW sky.

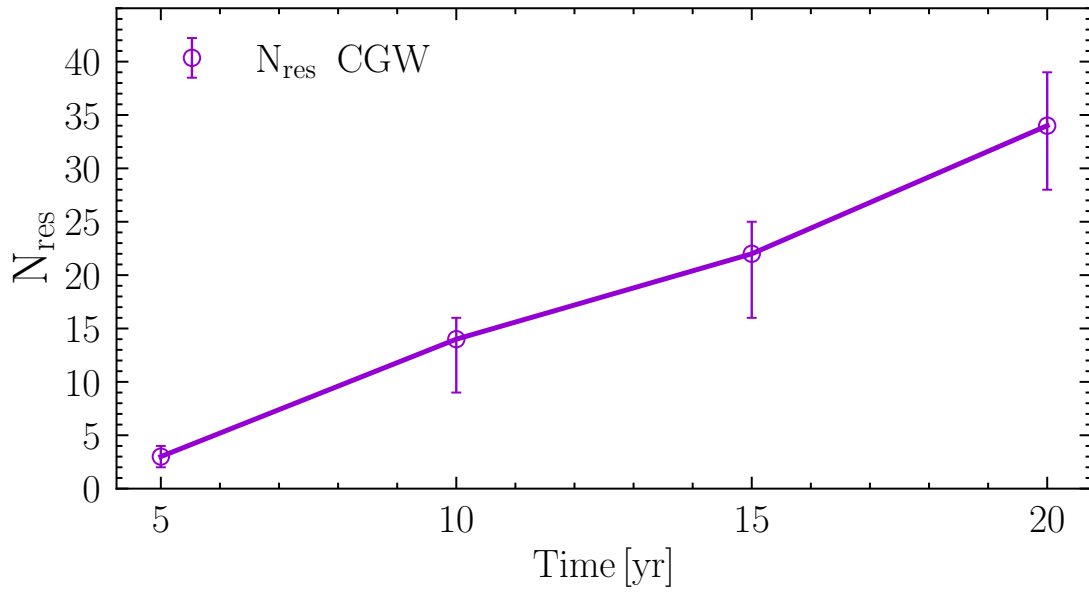


Figure 5: Predicted number of detectable single sources with SKAO-PTA. The open dots represent the median number of resolved continuous gravitational waves resolved from the 200 SMBHB populations, while error bars represent the 64 and 32 percentiles of the distribution.

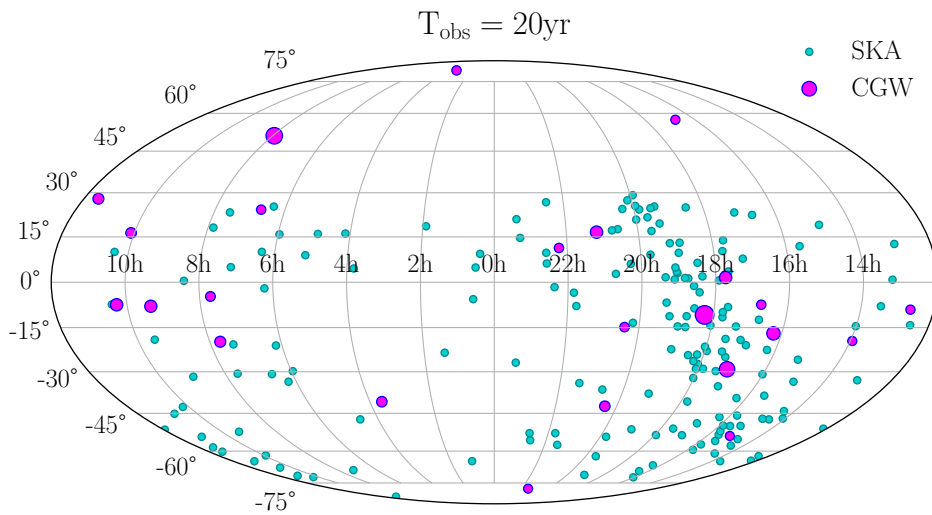


Figure 6: Sky distribution of the SKAO PTA pulsars (light-blue) and the SMBHBs detected as continuous gravitational waves (dark violet) in a single realization SMBHB population. The size of the dark violet points is weighted by the CGW S/N

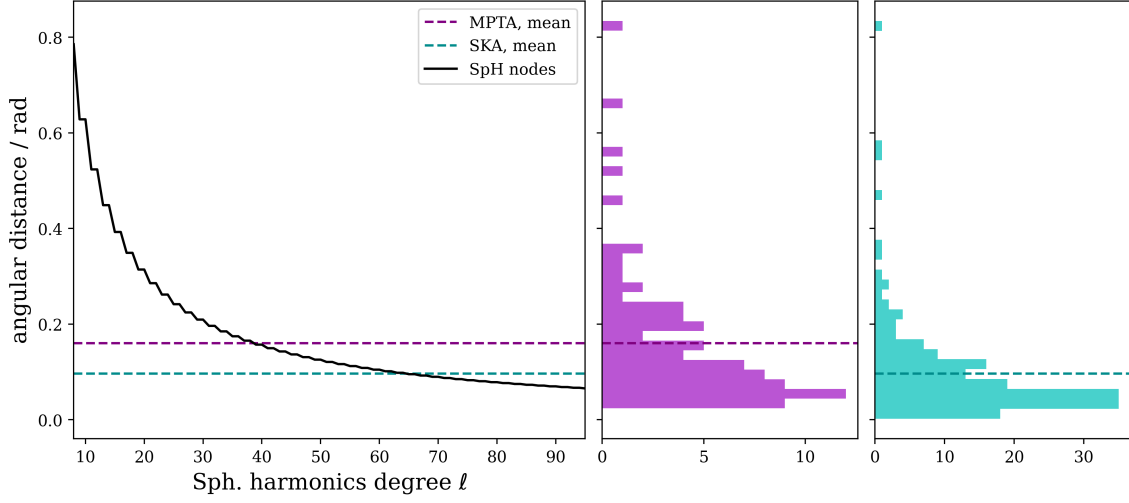


Figure 7: Maximum spherical harmonics degree locally constrainable by the MPTA and proposed SKAO PTA data sets, derived from the angular separations between the pulsars in the respective data sets. Left: Comparison between the minimum angular scale corresponding to the spherical harmonics degree ℓ (black curve) and the mean next-neighbour distance in the MPTA (purple line) and the SKAO PTA simulated from the MeerTime MSP census (teal line). Middle: Distribution of next-neighbour distances in the MPTA. Right: Distribution of next-neighbour distances in the proposed SKAO PTA.

To demonstrate the improvement that an SKAO PTA can yield compared to the currently operated MPTA, we assume that a potential GWB anisotropy analysis uses similar methods as the MPTA 4.5-year data set analysis (Grunthal et al., 2025).

As outlined by Pol et al. (2022); Grunthal et al. (2025), the maximum degree of spherical harmonics constrainable by a PTA of N_{PSR} pulsars can be estimated as $\ell_{\text{max}} = \text{floor}(\sqrt{N_{\text{PSR}}} - 1)$. Assuming the SKAO PTA containing 174 MSPs as described above, this means $\ell_{\text{max}}^{\text{SKA}} = 12$. This conservative, global resolution estimate indicates a significant improvement in angular resolution of the proposed SKAO PTA compared to the MPTA (83 pulsars, $\ell_{\text{max}}^{\text{MPTA}} = 8$).

The resolution potential of the SKAO PTA becomes even more visible using the more realistic estimate strategy developed by Grunthal et al. (2026), which simultaneously respects the diffraction limit of a PTA (i.e., the finite number of pulsars), while accounting for the changing density of pulsars across the sky. Fig. 7 shows that the pulsar-pair separation distribution of the SKAO PTA (right) allows for a local resolution corresponding to a spherical harmonics expansion up to $\ell_{\text{max}} = 65^2$. This corresponds to a mean local angular resolution of 2.7° , a factor of ~ 2 better than the local angular resolution of the MPTA (5.8°) (Grunthal et al., 2026).

Finally, the sky distribution of the point-spread-areas (PSA) of the SKAO PTA compared to the MPTA underline the significant step ahead an SKAO PTA would pose for the calculation of GW sky maps in the nanohertz regime. Fig. 8 shows the PSA distribution for white-noise-only simulations of both the MPTA and the above described SKAO PTA. Each data set spans 4.5 years, and both

²As outlined in Grunthal et al. (2026), this higher ℓ_{max} implies regularizing the Fisher matrix inversion following the scheme described in Grunthal et al. (2025), including not more than its first 174 singular values.

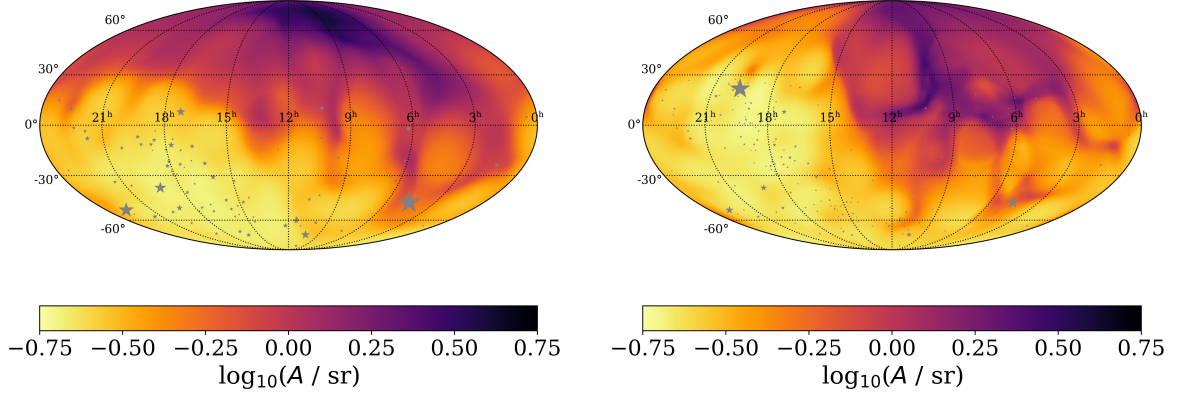


Figure 8: Spread of a point-source (point-spread-area) function of the sky position. Left: A simulated 4.5-year MeerKAT PTA data set. Right: A simulated 4.5-year SKAO PTA data set, with timing precisions based on the MeerTime MSP census. Both simulations assume white noise is the only noise source present in the observations.

maps were calculated with $\ell_{\max} = 8$ and a singular value cutoff of $n_{\text{SV}} = 32$, these values were inherited from the MPTA 4.5-year anisotropy analysis (Grunthal et al., 2025). Although the previous investigation has established that this is likely not the best parameter combination for calculating the best-scenario capabilities of the SKAO PTA, it enables a more direct comparison to the MPTA data set. It impressively shows the improvement the SKAO PTA can provide mapping the GW sky compared to the MPTA: The area with comparably small PSAs has grown significantly, especially in the Northern Hemisphere, and the darker shaded area (least sensitivity) is smaller and more sensitive than for the MPTA. Simultaneously, the right plot in Fig. 8 underlines the inevitably outstanding role an SKAO PTA will pose for mapping the GW sky using the combined data sets of all regional PTAs. With no regional PTA providing a comparably sensitive data set for the Southern Hemisphere, the SKAO PTA will serve as an indispensable pillar of any meaningful global³ nanohertz GW sky map.

7 The role of SKA-Low telescope

While current PTA observing campaigns emphasize decimeter-wavelength timing for maximal raw precision, the low-frequency domain (50–350 MHz) accessible to the SKA-Low telescope will be indispensable for understanding the propagation effects and systematics that limit timing stability. While the SKA-Low telescope will enable an extensive array of science, as discussed in Tiburzi et al. (2026, this collection.), incorporating the SKA-Low telescope into PTA programs will bridge the gap between precision timing and propagation monitoring, providing direct leverage on chromatic delays, pulse-shape evolution, and DM variability—dominant contributors to the single-pulsar noise budget.

Low-frequency pulsar studies with LOFAR and NenuFAR at, respectively, 100 to 200 MHz and < 100 MHz have already demonstrated this capability (Porayko et al., 2019; Donner et al., 2019; Tiburzi et al., 2019; Donner et al., 2020; Bondonneau et al., 2021; Tiburzi et al., 2021; Wu et al.,

³meaning balanced sensitivities on the Northern and Southern Hemisphere.

2022; Porayko et al., 2023; Susarla et al., 2024; Iraci et al., 2025). These efforts show that high-cadence campaigns at low radio-frequencies can reconstruct the DM and scattering structure of the IISM with sub- 10^{-5} pc cm $^{-3}$ precision, constraining stochastic plasma variations that would otherwise contaminate red-noise processes or mimic a GWB signal. Observational studies of pulsar sightlines and local IISM structures have likewise emphasized the need to characterize turbulence, bow shocks, and discrete ionized regions along the line of sight (Ocker et al., 2020, 2024a,b).

The Murchison Widefield Array (MWA) has demonstrated precise DM measurements and scintillation studies of bright southern MSPs (Bhat et al., 2016, 2018; Kaur et al., 2019, 2022). Until recently, the limited real-time capability of the array restricted its monitoring cadence, but an ongoing upgrade (Morrison et al., 2023) will soon enable continuous beamformed observations. Targeted campaigns on the bright MSP PSR J2241–5236 have already achieved DM precisions of $\sim 10^{-6}$ pc.cm $^{-3}$ by exploiting a flexible system design (Kaur et al., 2019). Contemporaneous observations with the uGMRT and Parkes, which span 70 MHz to 4 GHz, have demonstrated the importance of disentangling profile evolution from chromatic DM effects (Kaur et al., 2022). Recent work (Lee et al., 2025) indicates that a large fraction of southern-sky PTA pulsars are detectable with MWA, offering excellent prospects for high-cadence, low-frequency monitoring that will complement SKA-Low and provide legacy datasets for future PTA analyses. In the full AA4 configuration, the SKA-Low telescope will push these capabilities to their ultimate limit, reaching DM precisions near 10^{-8} pc cm $^{-3}$ (Tiburzi et al., 2026), a benchmark that will redefine low-frequency timing and propagation monitoring within PTA experiments.

Complementary progress at higher frequencies demonstrates that the DM precision can be improved even further through instantaneous dual-band (300–500 MHz and 1260–1460 MHz) observations, as shown with the SKA pathfinder uGMRT (Tarafdar et al., 2022; Rana et al., 2025). Joint analysis across this wide frequency range—using both narrow-band (Krishnakumar et al., 2021) and wideband (Paladi et al., 2024) DM estimation techniques—achieves order-of-magnitude gains in precision when the SKA-Low and the SKA-Mid telescopes observe simultaneously.

Parallel efforts within PTA collaborations are already advancing this integration. LOFAR and NenuFAR data are now incorporated into EPTA-InPTA analyses, with a dedicated LOFAR–EPTA program included in the second EPTA data release (Iraci et al., 2025), while CHIME provides complementary coverage (Agazie et al., 2025b) to the NANOGrav collaboration. The third data release of the IPTA will present results from the first combination of data from LOFAR, NENUFAR, uGMRT, and CHIME. The synergy among SKA-Low and current high- and low-frequency instruments will deliver a contiguous frequency baseline spanning more than an order of magnitude, enabling detailed modeling of pulse-profile evolution and DM transfer functions. This information will be essential for precise chromatic calibration and for disentangling GW and propagation-induced noise.

However, realizing the full scientific potential of low-frequency timing requires accurate modeling of frequency-dependent pulse-shape evolution and chromatic timing residuals by Donner et al. (2019) and Donner et al. (2020). Their analyses showed that LOFAR’s large fractional bandwidth can isolate intrinsic pulse evolution from propagation-induced effects, while complementary studies (e.g., Lam et al., 2016a) have quantified DM variability and scattering-induced distortions at low

frequencies. The SKA-Low telescope, with its greater sensitivity and continuous bandwidth, will extend this capability to a far larger pulsar sample, enabling direct, high-cadence tracking of chromatic delays within each PTA epoch.

In addition, the SKA-Low telescope’s large instantaneous bandwidth and sensitivity will permit direct measurement of scattering transfer functions at the same cadence as PTA timing, allowing correction of stochastic, frequency-dependent effects that otherwise masquerade as excess timing noise. These capabilities—repeatedly highlighted in multi-band calibration studies (Lam et al., 2016a; Donner et al., 2020; Tiburzi et al., 2021; Singha et al., 2024; Susarla et al., 2024)—will be further enhanced by coordinated observations across SKA-Low, uGMRT, CHIME, and SKA-Mid, enabling direct tests of DM structure functions on astronomical-unit scales and linking PTA noise budgets to measurable IISM dynamics (Wu et al., 2023).

Beyond IISM diagnostics, SKA-Low will enhance PTA science by extending timing baselines for bright southern pulsars that saturate higher-frequency receivers, improving spectral separation between chromatic and achromatic noise components. In concert with SKA-Mid, SKA-Low will thus provide the full frequency lever arm needed to isolate the nanohertz GWB from propagation-induced systematics (Verbiest et al., 2024). This precision will be crucial for advanced searches for individual SMBHBs (Ferranti et al., 2025) and for detecting anisotropy in the GWB (Pol et al., 2022; Gersbach et al., 2025a,b; Grunthal et al., 2025; Moreschi et al., 2025).

8 The role of very long baseline interferometry and use of the pulsar term

The SKAO is expected to measure accurate pulsar distances through pulsar timing, and the pulsar term can be incorporated in data analysis to improve the localization accuracy of single GW sources (Lee et al., 2011). Recent theoretical and simulation studies have further demonstrated that incorporating precise pulsar distance information from external measurements, such as very long baseline interferometry (VLBI), can dramatically enhance the localization accuracy of individual CGWs in PTA experiments. For example, Kato and Takahashi (2023) showed that, even if precise distance information with an accuracy of ~ 1 pc, comparable to the GW wavelength, is available for only a small subset of pulsars, rather than all pulsars, the sky localization of a single GW source can improve by more than an order of magnitude. This effect arises because precise distance information which is independent of timing observations allows the phase of the pulsar term in the GW signal to be tightly constrained, thereby breaking degeneracies between the source position and other parameters.

Building on this, Kato and Takahashi (2026) performed simulations with realistic sky distributions and actual distances for 87 IPTA pulsars. They assumed distance precisions of 0.37 pc and 1.7 pc for the two nearby pulsars PSRs J0437–4715 and J0030+0451, respectively, based on the precision levels anticipated with VLBI astrometry using the SKAO and assumed white noise levels for each pulsar of $\sigma_n = 30$ ns. It was demonstrated that the GW source localization improves by two orders of magnitude near J0437–4715 and by more than one order near J0030+0451, with substantial improvement maintained over a broader region of the sky (Fig. 9). These findings underline that even a limited set of high-precision pulsar distances can have a transformative impact on

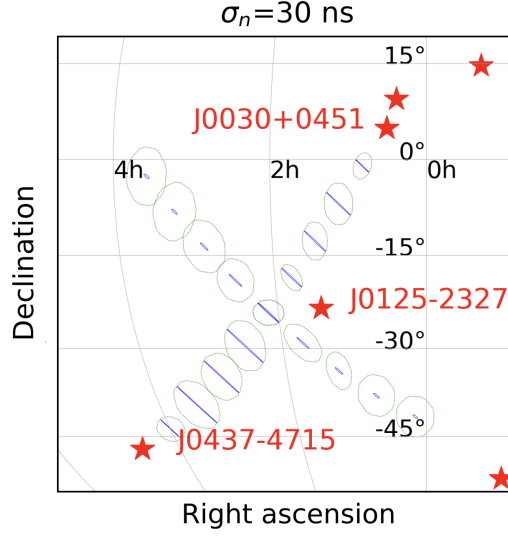


Figure 9: Expected localization precision (8σ) of a single GW source around two pulsars, J0437-4715 and J0030+0451 (Kato and Takahashi, 2026). Source localizations are shown at different assumed positions. The outer contours (green dashed line) correspond to the case without distance information, while the inner contour (blue solid line) correspond to the case with distance errors expected in the SKA era. The analysis assumes timing precision of $\sigma_n = 30$ ns can be achieved. The red stars show the positions of pulsars.

the capability of PTAs to pinpoint GW sources, facilitate host galaxy identification, and enable multi-messenger follow-up observations. These results highlight the exceptional synergy between high-precision VLBI astrometry and SKAO PTA science, strongly motivating the prioritization of distance measurements for the most influential pulsars in the array.

9 Connections to high-energy pulsar timing

Pulsar timing array efforts can also benefit from high energy observations of gamma-ray or X-ray bright MSPs. Millisecond pulsars emit prodigious high-energy emission, with more than 140 known to be gamma-ray bright (Smith et al., 2023). There are ongoing efforts to use observations of MSPs from the Fermi Large Area Telescope (Fermi-LAT) to search for gravitational waves (FERMI-LAT Collaboration et al., 2022), which have timing baselines extending to shortly after the launch of Fermi in 2008, as part of the Gamma-ray PTA (GPTA). Using a 12.5 year data set, the 95% limit on the amplitude of a GWB is $A_{\text{yr}} < 10^{-14}$. The GPTA is expected to be sensitive to CURN at an amplitude of $A_{\text{yr}} = 2 \times 10^{-15}$ with ≈ 26 yr observation, assuming the weak signal scaling $A_{\text{yr}} \propto T^{-13/6}$ (FERMI-LAT Collaboration et al., 2022). While there are pulsars that are common between radio and gamma-ray PTAs, many of the brightest gamma-ray MSPs are faint radio sources. The inclusion of gamma-ray bright MSPs can increase the size and sensitivity of international efforts.

A handful of MSPs can also be timed with adequate precision for GW searches using X-ray timing, as demonstrated by the NICER mission (Deneva et al., 2019). Past searches have detected red noise in X-ray observations of PSR J1824-2452A (Hazboun et al., 2022a), and current analyses show

evidence for red noise in X-ray data from the first MSP discovered, PSR J1939+2134 (K. Wayt, et al. in prep).

Even if a pulsar’s timing precision makes it better suited to PTA searches at radio wavelengths, gamma-ray and X-ray observations can help with better noise characterization. High-energy observations are not impacted by propagation effects through intervening plasma (discussed in Section 5) that impact timing observations at radio frequencies. Thus, the joint study of pulsars at high energies and radio can be used to better characterize chromatic noise processes and distinguish them from achromatic processes, including gravitational waves and intrinsic spin noise (Kerr et al., 2015). The detection of red noise in NICER MSP observations, confirms that the noise is intrinsic to these pulsars and not a misspecified chromatic noise.

Gamma-ray observations can also be used to understand the origin and impact of profile variability on pulsar timing. The gamma-ray emission mechanism, while likely related to radio emission, is different as it is more directly linked to the acceleration of charged particles (Harding et al., 2005). There has been no evidence for temporal variability in the gamma-ray emission of MSPs (Kerr, 2025); therefore, high-energy observations can be used to understand the nature of profile variability observed at radio wavelengths.

Observing pulsars in gamma-rays is fundamentally different than in radio. To produce pulse profiles with signal to noise ratios $\gg 1$ from gamma-ray photons requires days to months integration time. However, instruments such as Fermi-LAT have wide fields of view of \sim steradian, so monitoring of gamma-ray pulsars can be conducted commensal to survey observations. Additionally, “photon-by-photon” timing techniques (Kerr, 2011; Clark et al., 2015; FERMI-LAT Collaboration et al., 2022) provide a more optimal approach to using gamma-ray data than traditional (radio-like) TOA-based modeling. Both the traditional and photon-by-photon methods were used in the first GPTA GW searches.

Gamma-ray PTA sensitivity will steadily improve with the Fermi-LAT’s continued operation. The SKAO PTA will benefit greatly from contemporaneous gamma-ray, X-ray, and radio pulsar timing observations to better characterize both intrinsic and ISM-induced red noise processes, thereby improving the PTA’s sensitivity to the nHz GWB.

10 Requirements for the SKAO PTA

There are a number of key capabilities that are required to make the best use of the SKAO as a PTA instrument.

- **Observing bands:** Because increased bandwidths minimize system temperature fluctuations and improve sensitivity, the precision to which a pulsar can be timed is determined in part by the available simultaneous bandwidth. As steep-spectrum emitters, most MSPs perform best at relatively low radio frequencies; current PTA experiments conduct most observations between \sim 400 MHz and 4 GHz, though some instruments (such as LOFAR) significantly improve low-frequency coverage. Ultra-wideband receivers improve timing precision not only through increased bandwidth, but also by providing a simultaneous lever arm for characterizing and mitigating dispersion and scattering by the IISM. Such an ultra-wideband receiver

covering SKA-Mid bands 1-4 (or 5) would be ideal. Barring that, monitoring in bands 1 and 2 (350-1760 MHz) is a baseline requirement for PTA science.

- **Timing Precision:** Pulsars timed to better than $1\mu\text{s}$ precision are generally considered to improve sensitivity to the GWB (Siemens et al., 2013). Although the SKAO will facilitate significantly better precision (\sim tens of ns) for bright sources, PTA sensitivity has a strong (linear) dependence on the number of pulsars timed, suggesting that the SKAO PTA will include plenty of $1\mu\text{s}$ MSPs. Increased bandwidth, increased integration times (up to the jitter limit), high-quality polarization calibration, and improved system temperature are important contributions to the achievable timing precision.
- **Polarization fidelity:** High-quality polarimetry enables the use of full Stokes information in pulsar timing, which could result in higher timing precision (van Straten, 2013; Curyło et al., 2026). If uncorrected non-orthogonalities of the feed of even 0.2% and differential gain errors of 0.15% can introduce systematic timing errors of 100 ns (van Straten, 2006). Because polarization systematics introduced at the instrument level are correlated between all observed pulsars, controlling these effects can yield significant improvements not only in sensitivity, but also PTA performance. Regular observations of the pulsars themselves can be further used to improve polarization calibration, and may somewhat reduce the polarization purity requirements (van Straten, 2013). PTA observations will be taken with pulsars observed at antenna boresight, so on-axis polarization performance is of most importance.
- **Spectral purity:** Leakage between spectral channels can introduce frequency-dependent artefacts and cause bias in integrated pulse profiles that significantly hamper high-precision timing. MeerKAT has critically sampled coarse channels. For pulsar timing modes it was necessary to develop sharply tapered filters for MeerKAT, which reduced throughput close to the channel edges. This removed the artefacts while only reducing sensitivity by 5% (Bailes et al., 2020). With its oversampled filters should not exhibit such artefacts.
- **RFI removal:** RFI contamination decreases usable bandwidth and introduces other systematics that reduce the sensitivity of PTA observations. In addition to observatory-side improvements such as coordinated spectrum management, modernizing RFI excision algorithms could have a significant impact on PTA timing precision.
- **Overlap with MeerKAT:** It is essential to have time overlap of PTA observations between the SKA-Mid telescope and with MeerKAT, which will enable offsets between the two observatories to be measured. Offsets will likely be present in digital and analogue portions of the system. Different responses of MeerKAT and SKAO receiving systems can potentially result in different observed pulse profiles. It may be possible to measure absolute offsets by correlating sky noise (NANOGrav Collaboration et al., 2015) or observations of Giant pulses in pulsars, such as the Crab pulsar (Susobhanan et al., 2021). Overlapping (and simultaneous) observations will verify the timing performance of SKAO.
- **Ability to record data with multiple backends simultaneously.** Ancillary science would benefit from data being recorded in multiple modes. Single pulse analysis can be undertaken in base-band (voltage) format or in search mode (filterbank) format. Such studies are useful for both

understanding the nature of pulsar emission, but also for developing techniques to mitigate the effects of jitter noise. Scintillation studies often benefit from higher frequency resolution than possible or desired in pulsar timing observations, or the use of cyclic spectroscopy (Demorest, 2011) to deconvolve pulse profiles.

Post processing:

- Pulsar timing observations are relatively computationally inexpensive. Only one or a few tied array beams need to be formed. Phase resolved pulse profiles can be integrated together for many seconds without impacting science goals of the SKAO-PTA, with science data products produced without requiring significant resources from the science data processor.
- Wide-band timing methods: Because pulse profiles evolve as a function of frequency, extracting TOAs from averaged profiles can result in measurement biases. Wide-band timing techniques, which use a frequency-dependent template to measure one or more TOAs per epoch, improve timing precision and reduce the required number of timing parameters when wide-bandwidth systems are in use (Pennucci et al., 2014; Liu et al., 2014; Curyło et al., 2023; Paladi et al., 2024).
- Noise analysis and GW searches will use Bayesian codes (e.g., Lentati et al., 2014; Ellis et al., 2020) to search for GW signals and characterize the noise in the data set. These codes will be accelerated by hardware algorithm advances, as has been evidenced by increases in code speed in the 2020s. These models are developed in concert with pulsar timing models developed in codes such as TEMPO2 (Hobbs et al., 2006) or PINT (Luo et al., 2021). Given the sensitivity of the observations, it will be essential to continue to refine noise models. This could be through for example, looking at the DMCalc method (Krishnakumar et al., 2021; Rana et al., 2025) for estimating dispersion measures.

11 Connections to other SKAO science and other 2030 facilities

The large scale pulsar survey with SKAO (Keane et al., 2026) will help enlarge the pulsar sample for the SKAO PTA thereby making it the most sensitive PTA experiment. The projections in sensitivity provided above are based on the MSP population visible to SKA as of ~2020. The regular cadence monitoring over long time baseline needed for an SKAO PTA will have benefits for other pulsar science. While the measurements of variations in DM, scatter broadening, and solar wind over such time baseline will provide a better understanding of the IISM (Tiburzi et al., 2026), the estimate of timing noise will provide constraints for the structure of neutron star interiors (Dong et al., 2026; Basu et al., 2026). PTA observations will similarly contribute to NS mass measurements through new or improved Shapiro delay measurements. The jitter noise measurements over a wide frequency range will have implications for understanding the physics of the pulsar emission mechanism and magnetosphere (Oswald et al., 2026). Additional constraints on magnetospheric physics will come from wideband observations of profile change events in some PTA MSPs. Overall, precision timing of MSPs may also be helpful in tests for gravitational theory (Krishnan et al., 2026) apart from constraints on the existence dipolar gravitational radiation and alternative polarizations in

alternative gravity theories. These connections to other pulsar science with the SKA observatory are discussed in detail in the companion articles in this book.

Other next-generation radio instruments, such as the Deep Synoptic Array (DSA; formerly DSA-2000) and the next-generation Very Large Array (ngVLA), will be complementary to the SKA effort and further improve the GW sensitivity of IPTA data sets. Currently, the DSA project (Hallinan et al., 2019) plans to dedicate $\sim 25\%$ of on-sky time towards the observation of 150–200 MSPs for PTA science, with observations beginning in 2028. Spanning a bandwidth of 700 MHz–2 GHz, the instrument will operate in an ideal range for radio pulsar observations and provide a substantial sensitivity and timing precision boost, especially for Northern hemisphere pulsars (with a declination limit of -39 degrees). On a longer timescale, the ngVLA (Chatterjee, 2018) is slated to provide higher-frequency, high-sensitivity capabilities to PTAs — which lessen the impact of IISM effects — and support synergistic long-baseline science as described in Section 8. These instruments, taken together with the SKAO, will provide the full-sky coverage necessary to maximize sensitivity to the GWB and other signal sources.

Several other 2030 facilities will be complementary to the SKAO PTA. The Laser Interferometer Space Antenna (LISA) is an ESA-NASA mission to launch a space-based GW observatory. LISA will open a new window on the millihertz GW frequency band and is slated to launch in 2035 (Colpi et al., 2024). Other missions, including TianQin (Luo et al., 2025) and Taiji (Ruan et al., 2020) are planned on a similar timescale. This millihertz GW band will provide a complementary view on the evolution and growth of SMBHBs across cosmic time by capturing GWs from the mergers themselves (Rhook and Wyithe, 2005; Sesana et al., 2011; Klein et al., 2016; Katz et al., 2020; Barausse et al., 2020; Toubiana et al., 2025). The potential of multiband SMBHB observations is already being explored with forecasting of LISA detection rates based on current PTA constraints on the SMBHB population (e.g. Steinle et al., 2023). Detections of GWBs in multiple bands can potentially to understand the physical processes that cause inflation (Lasky et al., 2016). Distinguishing between multiple sources of a cosmological GWB will require coordinated activities, combining PTA measurements with observations of the cosmic microwave background, and future ground and space-based gravitational wave detectors such as Cosmic Explorer (Evans et al., 2021), the Einstein Telescope (Punturo et al., 2010) and LISA (Colpi et al., 2024).

12 Conclusions

The SKAO promises to be an excellent vehicle for an efficient and high impact PTA experiment. The sensitivity, wide frequency coverage and availability of sub-arrays will ensure it can be optimized to maximize nanohertz-frequency GW science in the 2030s and beyond. Through the SKAO Pulsar Timing Array it will be able to make detailed maps of the nanohertz-frequency gravitational wave sky, and use them to chart the nature of gravitational wave sources, and the fundamental physics that powers the emission.

Acknowledgements

Part of this work was undertaken as part of the Australian Research Council Centre of Excellence for Gravitational Wave Discovery (OzGrav) CE230100016. HTC acknowledges support from the U.S. Naval Research Laboratory. Basic research in pulsar astronomy at NRL is supported by NASA, in particular via Fermi Guest Investigator award NNG22OB35A. AG acknowledges support of the Department of Atomic Energy, Government of India, under Project Identification No. RTI 4002 KG acknowledges support from the International Max Planck Research School (IMPRS) for Astronomy and Astrophysics at the Universities of Bonn and Cologne and the Bonn-Cologne Graduate School of Physics and Astronomy. All authors affiliated with the Max-Planck-Gesellschaft (MPG) acknowledge its constant support. JSH acknowledges support from NSF CAREER award 2339728 and NSF Physics Frontiers Center award 2020265. JSH, MTM and CMFM acknowledge support from the NANOGrav Collaboration's National Science Foundation (NSF) Physics Frontiers Center award 2020265. BCJ acknowledges the support from Raja Ramanna Chair fellowship of the Department of Atomic Energy, Government of India (RRC – Track I Grant 3/3401 Atomic Energy Research 00 004 Research and Development 27 02 31 1002//2/2023/RRC/R&D-II/13886 and 1002/2/2023/RRC/R&D-II/14369). RK is supported by JSPS KAKENHI Grant Number 24K17051. KJL is supported by the National SKA Program of China (Grant No. 2020SKA012010). HM is supported by the UK Space Agency, Grant No. ST/V002813/1. MTM and CMFM acknowledge support from the NANOGrav Collaboration's National Science Foundation (NSF) Physics Frontiers Center award 1430284. CMFM was also supported in part by the NSF under Grant NSF PHY-1748958 and NASA LPS 80NSSC24K0440 AP acknowledges financial support from the European Research Council (ERC) starting grant 'GIGA' (grant agreement number: 101116134) and through the NWO-I Veni fellowship. GMS acknowledges the financial support provided under the European Union's H2020 ERC Consolidator Grant B Massive (Grant Agreement: 818691) and Advanced Grant PINGU (Grant Agreement: 101142097). KT is partially supported by JSPS KAKENHI Grant Numbers 20H00180, 21H01130, 21H04467, and 24H01813, and Bilateral Joint Research Projects of JSPS. XX is funded by the grant CNS2023-143767. Grant CNS2023-143767 is funded by MICIU/AEI/10.13039/501100011033 and by European Union NextGenerationEU/PRTR. IFAE is partially funded by the CERCA program of the Generalitat de Catalunya.

References

- A. G. Abac et al. *Phys. Rev. L.*, 135(11):111403, Sept. 2025. doi: 10.1103/kw5g-d732.
- B. P. Abbott et al. *Phys. Rev. L.*, 116(6):061102, Feb. 2016. doi: 10.1103/PhysRevLett.116.061102.
- B. P. Abbott et al. *Annalen der Physik*, 529(1-2):1600209, Jan. 2017a. doi: 10.1002/andp.201600209.
- B. P. Abbott et al. *Phys. Rev. L.*, 119(16):161101, Oct. 2017b. doi: 10.1103/PhysRevLett.119.161101.
- B. P. Abbott et al. *ApJL*, 848(2):L12, Oct. 2017c. doi: 10.3847/2041-8213/aa91c9.

- F. Acernese et al. *Classical and Quantum Gravity*, 32(2):024001, Jan. 2015. doi: 10.1088/0264-9381/32/2/024001.
- A. Afzal et al. *ApJL*, 951(1):L11, July 2023. doi: 10.3847/2041-8213/acdc91.
- A. Afzal et al. *Astrophys. J. Lett.*, 951(1):L11, July 2023. doi: 10.3847/2041-8213/acdc91.
- N. Agarwal et al. *arXiv e-prints*, art. arXiv:2508.16534, Aug. 2025. doi: 10.48550/arXiv.2508.16534.
- G. Agazie et al. *ApJL*, 951(1):L9, July 2023a. doi: 10.3847/2041-8213/acda9a.
- G. Agazie et al. *ApJL*, 951(1):L8, July 2023b. doi: 10.3847/2041-8213/acdac6.
- G. Agazie et al. *ApJL*, 951(2):L50, July 2023c. doi: 10.3847/2041-8213/ace18a.
- G. Agazie et al. *ApJL*, 951(1):L10, July 2023d. doi: 10.3847/2041-8213/acda88.
- G. Agazie et al. *ApJ*, 966(1):105, May 2024a. doi: 10.3847/1538-4357/ad36be.
- G. Agazie et al. *ApJ*, 963(2):144, Mar. 2024b. doi: 10.3847/1538-4357/ad1f61.
- G. Agazie et al. *ApJ*, 978(1):31, Jan. 2025a. doi: 10.3847/1538-4357/ad93d5.
- G. Agazie et al. *arXiv e-prints*, art. arXiv:2510.16668, Oct. 2025b. doi: 10.48550/arXiv.2510.16668.
- T. Akutsu et al. *Progress of Theoretical and Experimental Physics*, 2021(5):05A103, May 2021. doi: 10.1093/ptep/ptaa120.
- Y. Ali-Haïmoud, T. L. Smith, and C. M. F. Mingarelli. *Phys. Rev. D*, 102(12):122005, Dec. 2020. doi: 10.1103/PhysRevD.102.122005.
- Y. Ali-Haïmoud, T. L. Smith, and C. M. F. Mingarelli. *Phys. Rev. D*, 103(4):042009, Feb. 2021. doi: 10.1103/PhysRevD.103.042009.
- B. Allen. In *Les Houches School of Physics: Astrophysical Sources of Gravitational Radiation*, pages 373–417, 4 1996.
- B. Allen and E. P. S. Shellard. *Phys. Rev. D*, 45:1898–1912, 1992. doi: 10.1103/PhysRevD.45.1898.
- B. Allen et al. *arXiv e-prints*, art. arXiv:2304.04767, Apr. 2023. doi: 10.48550/arXiv.2304.04767.
- M. A. Alpar, A. F. Cheng, M. A. Ruderman, and J. Shaham. *Nature*, 300(5894):728–730, Dec. 1982. doi: 10.1038/300728a0.
- P. Amaro-Seoane et al. *MNRAS*, 402(4):2308–2320, Mar. 2010. doi: 10.1111/j.1365-2966.2009.16104.x.
- K. N. Ananda, C. Clarkson, and D. Wands. *Phys. Rev. D*, 75:123518, 2007. doi: 10.1103/PhysRevD.75.123518.
- J. W. Armstrong, B. J. Rickett, and S. R. Spangler. *ApJ*, 443:209, Apr. 1995. doi: 10.1086/175515.

- A. Arvanitaki, J. Huang, and K. Van Tilburg. *Phys. Rev. D*, 91(1):015015, 2015. doi: 10.1103/PhysRevD.91.015015.
- Z. Arzoumanian et al. *ApJ*, 859:47, May 2018. doi: 10.3847/1538-4357/aabd3b.
- Z. Arzoumanian et al. *ApJL*, 905(2):L34, Dec. 2020a. doi: 10.3847/2041-8213/abd401.
- Z. Arzoumanian et al. *ApJ*, 900(2):102, Sept. 2020b. doi: 10.3847/1538-4357/ababa1.
- P. Athron, C. Balazs, D. Jacobson, and Y.-L. S. Wu. *Physical Review Letters*, 132(22):221001, 2024. doi: 10.1103/PhysRevLett.132.221001.
- D. C. Backer. *Nature*, 228(5278):1297–1298, Dec. 1970. doi: 10.1038/2281297a0.
- D. C. Backer et al. *Nature*, 300(5893):615–618, Dec. 1982. doi: 10.1038/300615a0.
- J. G. Baier, J. S. Hazboun, and J. D. Romano. *Classical and Quantum Gravity*, 42(7):075008, Apr. 2025. doi: 10.1088/1361-6382/adbbab.
- M. Bailes et al. *PASA*, 37:e028, July 2020. doi: 10.1017/pasa.2020.19.
- E. Barausse et al. *ApJ*, 904(1):16, Nov. 2020. doi: 10.3847/1538-4357/abba7f.
- A. Basu et al. arXiv search: Report number AASKAII/AvishekBasu01, 2026.
- D. Baumann, P. Steinhardt, K. Takahashi, and K. Ichiki. *Phys. Rev. D*, 76(8):084019, Oct. 2007. doi: 10.1103/PhysRevD.76.084019.
- M. C. Begelman, R. D. Blandford, and M. J. Rees. *Nature*, 287(5780):307–309, Sept. 1980. doi: 10.1038/287307a0.
- N. D. R. Bhat et al. *ApJ*, 818(1):86, Feb. 2016. doi: 10.3847/0004-637X/818/1/86.
- N. D. R. Bhat et al. *ApJSS*, 238(1):1, Sept. 2018. doi: 10.3847/1538-4365/aad37c.
- M. K. Bird, E. Schrufer, H. Volland, and W. Sieber. *Nature*, 283:459–460, Jan. 1980. doi: 10.1038/283459a0.
- D. Blas, D. L. Nacir, and S. Sibiryakov. *Phys. Rev. L.*, 118(26):261102, 2017. doi: 10.1103/PhysRevLett.118.261102.
- L. Bondonneau et al. *A&A*, 652:A34, Aug. 2021. doi: 10.1051/0004-6361/202039339.
- L. Boyle and U.-L. Pen. *Phys. Rev. D*, 86(12):124028, Dec. 2012. doi: 10.1103/PhysRevD.86.124028.
- L. A. Boyle and P. J. Steinhardt. *Phys. Rev. D*, 77:063504, 2008. doi: 10.1103/PhysRevD.77.063504.
- R. N. Caballero et al. *MNRAS*, 481(4):5501–5516, Dec. 2018. doi: 10.1093/mnras/sty2632.
- Y.-F. Cai, S. Pi, and M.-Z. Wang. *JCAP*, 2021(09):008, 2021. doi: 10.1088/1475-7516/2021/09/008.
- P. Campeti and E. Komatsu. *ApJ*, 941(2):110, Dec. 2022. doi: 10.3847/1538-4357/ac9ea3.

- C. Caprini and D. G. Figueroa. *Class. Quantum Gravity*, 35(16):163001, 2018. doi: 10.1088/1361-6382/aac608.
- C. Caprini, R. Durrer, and G. Servant. *JCAP*, 12:024, 2009. doi: 10.1088/1475-7516/2009/12/024.
- C. Caprini et al. *JCAP*, 03:024, 2020. doi: 10.1088/1475-7516/2020/03/024.
- A. Caputo et al. *Phys. Rev. D*, 100(6):063515, 2019. doi: 10.1103/PhysRevD.100.063515.
- J. Cardinal Tremblay et al. *ApJL*, 998(2):L42, Feb. 2026. doi: 10.3847/2041-8213/ae3c98.
- S. M. Carroll, G. B. Field, and R. Jackiw. *Phys. Rev. D*, 41:1231, 1990. doi: 10.1103/PhysRevD.41.1231.
- J. A. Casey-Clyde et al. *ApJ*, 987(2):106, July 2025. doi: 10.3847/1538-4357/adce05.
- A. Castillo et al. *JCAP*, 06(06):014, 2022. doi: 10.1088/1475-7516/2022/06/014.
- D. J. Champion, G. B. Hobbs, R. N. Manchester, et al. *ApJL*, 720:L201–L205, Sept. 2010. doi: 10.1088/2041-8205/720/2/L201.
- S. Chatterjee. In E. Murphy, editor, *Science with a Next Generation Very Large Array*, volume 517 of *Astronomical Society of the Pacific Conference Series*, page 751, Dec. 2018.
- S. Chen, A. Sesana, and W. Del Pozzo. *MNRAS*, 470(2):1738–1749, Sept. 2017. doi: 10.1093/mnras/stx1093.
- S. Chen et al. *MNRAS*, 508(4):4970–4993, Dec. 2021. doi: 10.1093/mnras/stab2833.
- S. Chen et al. *A&A*, 699:A165, July 2025. doi: 10.1051/0004-6361/202452550.
- S.-S. Chern and J. Simons. *Annals of Mathematics*, 99(1):48–69, 1974. ISSN 0003486X, 19398980.
- C. J. Clark et al. *ApJL*, 809(1):L2, Aug. 2015. doi: 10.1088/2041-8205/809/1/L2.
- C. J. Clark et al. *MNRAS*, 519(4):5590–5606, Mar. 2023. doi: 10.1093/mnras/stac3742.
- R. T. Co et al. *JCAP*, 2022(11):058, 2022. doi: 10.1088/1475-7516/2022/11/058.
- M. Colpi et al. *arXiv e-prints*, art. arXiv:2402.07571, Feb. 2024. doi: 10.48550/arXiv.2402.07571.
- J. M. Cordes and F. A. Jenet. *ApJ*, 752(1):54, June 2012. doi: 10.1088/0004-637X/752/1/54.
- J. M. Cordes and R. M. Shannon. *arXiv e-prints*, art. arXiv:1010.3785, Oct. 2010. doi: 10.48550/arXiv.1010.3785.
- J. M. Cordes et al. *New Astron. Rev.*, 48(11-12):1413–1438, Dec. 2004. doi: 10.1016/j.newar.2004.09.040.
- C. C. Counselman, III and J. M. Rankin. *ApJ*, 175:843, Aug. 1972. doi: 10.1086/151604.
- M. Curyło et al. *ApJ*, 944(2):128, Feb. 2023. doi: 10.3847/1538-4357/aca535.
- M. Curyło et al. *MNRAS*, May 2026. doi: 10.1093/mnras/stag835.
- S. Dandapat et al. *Phys. Rev. D*, 108(2):024013, July 2023. doi: 10.1103/PhysRevD.108.024013.

- S. Dandapat et al. *Phys. Rev. D*, 109(10):103018, May 2024. doi: 10.1103/PhysRevD.109.103018.
- P. B. Demorest. *MNRAS*, 416(4):2821–2826, Oct. 2011. doi: 10.1111/j.1365-2966.2011.19230.x.
- P. B. Demorest et al. *ApJ*, 762(2):94, Jan. 2013. doi: 10.1088/0004-637X/762/2/94.
- J. S. Deneva et al. *ApJ*, 874(2):160, Apr. 2019. doi: 10.3847/1538-4357/ab0966.
- S. Detweiler. *ApJ*, 234:1100–1104, Dec. 1979. doi: 10.1086/157593.
- L. Dey et al. *ApJ*, 866(1):11, Oct. 2018. doi: 10.3847/1538-4357/aadd95.
- G. Domènech. *Universe*, 7(11):398, 2021. doi: 10.3390/universe7110398.
- W. Dong et al. *MNRAS*, 545(4):staf2053, Feb. 2026. doi: 10.1093/mnras/staf2053.
- J. Y. Donner et al. *A&A*, 624:A22, Apr. 2019. doi: 10.1051/0004-6361/201834059.
- J. Y. Donner et al. *A&A*, 644:A153, Dec. 2020. doi: 10.1051/0004-6361/202039517.
- J. Y. Donner et al. *A&A*, 639:A77, 2020. doi: 10.1051/0004-6361/202039517.
- R. T. Edwards, G. B. Hobbs, and R. N. Manchester. *MNRAS*, 372(4):1549–1574, Nov. 2006. doi: 10.1111/j.1365-2966.2006.10870.x.
- J. Ellis, M. Lewicki, V. Vaskonen, and H. Veermäe. *A&A*, 685:A94, 2024. doi: 10.1051/0004-6361/202348224.
- J. A. Ellis, M. Vallisneri, S. R. Taylor, and P. T. Baker. ENTERPRISE: Enhanced Numerical Toolbox Enabling a Robust Pulsar Inference Suite, Sept. 2020.
- EPTA Collaboration et al. *A&A*, 678:A48, Oct. 2023a. doi: 10.1051/0004-6361/202346841.
- EPTA Collaboration et al. *A&A*, 678:A49, Oct. 2023b. doi: 10.1051/0004-6361/202346842.
- EPTA Collaboration et al. *A&A*, 685:A94, May 2024a. doi: 10.1051/0004-6361/202347433.
- EPTA Collaboration et al. *A&A*, 690:A118, Oct. 2024b. doi: 10.1051/0004-6361/202348568.
- EPTA+InPTA Collaboration et al. *A&A*, 678:A50, Oct. 2023. doi: 10.1051/0004-6361/202346844.
- J. R. Espinosa, D. Racco, and A. Riotto. *JCAP*, 09:012, 2018. doi: 10.1088/1475-7516/2018/09/012.
- M. Evans et al. *arXiv e-prints*, art. arXiv:2109.09882, Sept. 2021. doi: 10.48550/arXiv.2109.09882.
- M. Favata. *Classical and Quantum Gravity*, 27(8):084036, Apr. 2010. doi: 10.1088/0264-9381/27/8/084036.
- FERMI-LAT Collaboration et al. *Science*, 376(6592):521–523, Apr. 2022. doi: 10.1126/science.abm3231.
- I. Ferranti et al. *A&A*, 694:A38, Feb. 2025. doi: 10.1051/0004-6361/202452805.
- R. Z. Ferreira, A. Notari, O. Pujolas, and F. Rompineve. *JCAP*, 02:001, 2023. doi: 10.1088/1475-7516/2023/02/001.

- R. Z. Ferreira, A. Notari, and M. S. Sloth. *Phys. Rev. L.*, 132(17):171002, 2024. doi: 10.1103/PhysRevLett.132.171002.
- R. S. Foster and D. C. Backer. *ApJ*, 361:300, Sept. 1990. doi: 10.1086/169195.
- K. A. Gersbach et al. *arXiv e-prints*, art. arXiv:2509.07090, Sept. 2025a. doi: 10.48550/arXiv.2509.07090.
- K. A. Gersbach, S. R. Taylor, P. M. Meyers, and J. D. Romano. *Phys. Rev. D*, 111(2):023027, Jan. 2025b. doi: 10.1103/PhysRevD.111.023027.
- P. Gitika et al. *PASA*, 42:e146, Oct. 2025. doi: 10.1017/pasa.2025.10107.
- B. Goncharov et al. *MNRAS*, 502(1):478–493, Mar. 2021a. doi: 10.1093/mnras/staa3411.
- B. Goncharov et al. *ApJL*, 917(2):L19, Aug. 2021b. doi: 10.3847/2041-8213/ac17f4.
- B. Goncharov et al. *ApJL*, 932(2):L22, June 2022. doi: 10.3847/2041-8213/ac76bb.
- Y. Gouttenoire, G. Servant, and P. Simakachorn. *JCAP*, 07:032, 2020. doi: 10.1088/1475-7516/2020/07/032.
- L. P. Grishchuk. *Zhurnal Eksperimentalnoi i Teoreticheskoi Fiziki*, 67:825–838, Jan. 1974.
- L. P. Grishchuk. *Soviet Physics Uspekhi*, 20(4):319–334, Apr. 1977. doi: 10.1070/PU1977v020n04ABEH005327.
- E. J. Groth. *ApJSS*, 29:453–465, Nov. 1975. doi: 10.1086/190354.
- K. Grunthal et al. *MNRAS*, 536(2):1501–1517, Jan. 2025. doi: 10.1093/mnras/stae2573.
- K. Grunthal et al. *A&A*, 706:A352, Feb. 2026. doi: 10.1051/0004-6361/202557896.
- H.-K. Guo, K. Sinha, D. Vagie, and G. White. *JCAP*, 01:001, 2021. doi: 10.1088/1475-7516/2021/01/001.
- Y. J. Guo, K. J. Lee, and R. N. Caballero. *MNRAS*, 475(3):3644–3653, Apr. 2018. doi: 10.1093/mnras/stx3326.
- Y. J. Guo, G. Y. Li, K. J. Lee, and R. N. Caballero. *MNRAS*, 489(4):5573–5581, Nov. 2019. doi: 10.1093/mnras/stz2515.
- Y. J. Guo, R. N. Caballero, D. J. Champion, and K. J. Lee. *MNRAS*, 532(3):2943–2954, Aug. 2024. doi: 10.1093/mnras/stae1660.
- A. H. Guth. *Phys. Rev. D*, 23(2):347–356, Jan. 1981. doi: 10.1103/PhysRevD.23.347.
- G. Hallinan et al. In *Bulletin of the American Astronomical Society*, volume 51, page 255, Sept. 2019. doi: 10.48550/arXiv.1907.07648.
- A. K. Harding, V. V. Usov, and A. G. Muslimov. *ApJ*, 622(1):531–543, Mar. 2005. doi: 10.1086/427840.

- J. S. Hazboun, J. D. Romano, and T. L. Smith. *Phys. Rev. D*, 100(10):104028, Nov. 2019. doi: 10.1103/PhysRevD.100.104028.
- J. S. Hazboun et al. *ApJ*, 928(1):67, Mar. 2022a. doi: 10.3847/1538-4357/ac54ae.
- J. S. Hazboun et al. *ApJ*, 929(1):39, Apr. 2022b. doi: 10.3847/1538-4357/ac5829.
- R. W. Hellings and G. S. Downs. *ApJL*, 265:L39–L42, Feb. 1983. doi: 10.1086/183954.
- M. Hindmarsh, S. J. Huber, K. Rummukainen, and D. J. Weir. *Phys. Rev. Lett.*, 112:041301, 2014. doi: 10.1103/PhysRevLett.112.041301.
- M. Hindmarsh, M. Lüben, J. Lumma, and M. Pauly. *SciPost Physics Lecture Notes*, page 024, 2021. doi: 10.48550/arXiv.2008.09136.
- T. Hiramatsu, M. Kawasaki, and K. Saikawa. *JCAP*, 02:031, 2014. doi: 10.1088/1475-7516/2014/02/031.
- K. Hirata et al. *Phys. Rev. L.*, 58(14):1490–1493, Apr. 1987. doi: 10.1103/PhysRevLett.58.1490.
- G. Hobbs et al. *Classical and Quantum Gravity*, 27(8):084013, Apr. 2010. doi: 10.1088/0264-9381/27/8/084013.
- G. Hobbs et al. *MNRAS*, 427(4):2780–2787, Dec. 2012. doi: 10.1111/j.1365-2966.2012.21946.x.
- G. Hobbs et al. *MNRAS*, 491(4):5951–5965, Feb. 2020. doi: 10.1093/mnras/stz3071.
- G. B. Hobbs, R. T. Edwards, and R. N. Manchester. *MNRAS*, 369(2):655–672, June 2006. doi: 10.1111/j.1365-2966.2006.10302.x.
- C. J. Hogan. *MNRAS*, 218:629–636, Feb. 1986. doi: 10.1093/mnras/218.4.629.
- X.-S. Hu et al. *Phys. Rev. D*, 113(12):123019, June 2026. doi: 10.1103/wff3-b1fs.
- R. A. Hulse and J. H. Taylor. *ApJL*, 195:L51–L53, Jan. 1975. doi: 10.1086/181708.
- IceCube Collaboration et al. *Science*, 361(6398):147–151, July 2018. doi: 10.1126/science.aat2890.
- K. Inomata, K. Kohri, and T. Terada. *Phys. Rev. D*, 104(12):123525, 2021. doi: 10.1103/PhysRevD.104.123525.
- F. Iraci et al. *A&A*, 692:A170, Dec. 2024. doi: 10.1051/0004-6361/202450740.
- F. Iraci et al. *A&A*, 704:A109, Dec. 2025. doi: 10.1051/0004-6361/202555516.
- D. Izquierdo-Villalba, A. Sesana, S. Bonoli, and M. Colpi. *MNRAS*, 509(3):3488–3503, Jan. 2022. doi: 10.1093/mnras/stab3239.
- A. H. Jaffe and D. C. Backer. *ApJ*, 583(2):616–631, Feb. 2003. doi: 10.1086/345443.
- G. Janssen et al. In *Advancing Astrophysics with the Square Kilometre Array (AASKA14)*, page 37, Apr. 2015. doi: 10.22323/1.215.0037.
- R. J. Jennings et al. *ApJ*, 964(2):179, Apr. 2024. doi: 10.3847/1538-4357/ad2930.

- B. C. Joshi et al. *Journal of Astrophysics and Astronomy*, 43(2):98, Dec. 2022. doi: 10.1007/s12036-022-09869-w.
- M. Kamionkowski, A. Kosowsky, and M. S. Turner. *Phys. Rev. D*, 49:2837–2851, 1994. doi: 10.1103/PhysRevD.49.2837.
- R. Kato and K. Takahashi. *Phys. Rev. D*, 108(12):123535, Dec. 2023. doi: 10.1103/PhysRevD.108.123535.
- R. Kato and K. Takahashi. *Phys. Rev. D*, 113(2):022001, Jan. 2026. doi: 10.1103/4fyl-fzt8.
- M. L. Katz et al. *MNRAS*, 491(2):2301–2317, Jan. 2020. doi: 10.1093/mnras/stz3102.
- D. Kaur et al. *ApJ*, 882(2):133, Sept. 2019. doi: 10.3847/1538-4357/ab338f.
- D. Kaur et al. *ApJL*, 930(2):L27, May 2022. doi: 10.3847/2041-8213/ac64ff.
- E. F. Keane et al. arXiv search: Report number AASKAII/Keane01, 2026.
- L. Z. Kelley, L. Blecha, and L. Hernquist. *MNRAS*, 464(3):3131–3157, Jan. 2017. doi: 10.1093/mnras/stw2452.
- L. Z. Kelley et al. *MNRAS*, 477(1):964–976, June 2018. doi: 10.1093/mnras/sty689.
- M. Kerr. *ApJ*, 732(1):38, May 2011. doi: 10.1088/0004-637X/732/1/38.
- M. Kerr. *MNRAS*, 452(1):607–615, Sept. 2015. doi: 10.1093/mnras/stv1296.
- M. Kerr. *ApJ*, 991(2):225, Oct. 2025. doi: 10.3847/1538-4357/adfa95.
- M. Kerr et al. *ApJ*, 814(2):128, Dec. 2015. doi: 10.1088/0004-637X/814/2/128.
- M. Kerr et al. *ApJ*, 984(2):180, May 2025. doi: 10.3847/1538-4357/adc7a6.
- A. Khmelnitsky and V. Rubakov. *JCAP*, 02:019, 2014. doi: 10.1088/1475-7516/2014/02/019.
- N. M. Khusid et al. *ApJ*, 955(1):25, Sept. 2023. doi: 10.3847/1538-4357/ace16f.
- T. W. B. Kibble. *J. Phys. A*, 9:1387–1398, 1976. doi: 10.1088/0305-4470/9/8/029.
- S. Kiehlmann et al. *ApJ*, 985(1):59, May 2025. doi: 10.3847/1538-4357/adc567.
- T. Kikunaga et al. *PASA*, 41:e036, May 2024. doi: 10.1017/pasa.2024.30.
- H. Kim and A. Mitridate. *Phys. Rev. D*, 109(5):055017, 2024. doi: 10.1103/PhysRevD.109.055017.
- A. Klein et al. *Phys. Rev. D*, 93(2):024003, Jan. 2016. doi: 10.1103/PhysRevD.93.024003.
- B. Kocsis and A. Sesana. *MNRAS*, 411(3):1467–1479, Mar. 2011. doi: 10.1111/j.1365-2966.2010.17782.x.
- K. Kohri and T. Terada. *Phys. Rev. D*, 97(12):123532, 2018. doi: 10.1103/PhysRevD.97.123532.
- S. M. Kopeikin. *Phys. Rev. D*, 56(8):4455–4469, Oct. 1997. doi: 10.1103/PhysRevD.56.4455.

- J. Kormendy and L. C. Ho. *ARA&A*, 51(1):511–653, Aug. 2013. doi: 10.1146/annurev-astro-082708-101811.
- M. Kramer and D. J. Champion. *Classical and Quantum Gravity*, 30(22):224009, Nov. 2013. doi: 10.1088/0264-9381/30/22/224009.
- M. A. Krishnakumar et al. *A&A*, 651:A5, July 2021. doi: 10.1051/0004-6361/202140340.
- V. V. Krishnan et al. arXiv search: Report number AASKAII/VenkatramanKrishnan01, 2026.
- A. D. Kulkarni et al. *MNRAS*, 528(2):3658–3667, Feb. 2024. doi: 10.1093/mnras/stae041.
- A. D. Kulkarni, R. M. Shannon, D. J. Reardon, and M. T. Miles. *MNRAS*, 544(3):2795–2810, Dec. 2025. doi: 10.1093/mnras/staf1930.
- S. Kuroyanagi, T. Takahashi, and S. Yokoyama. *JCAP*, 02:003, 2015. doi: 10.1088/1475-7516/2015/02/003.
- S. Laine et al. *ApJL*, 894(1):L1, May 2020. doi: 10.3847/2041-8213/ab79a4.
- M. T. Lam. *ApJ*, 868(1):33, Nov. 2018. doi: 10.3847/1538-4357/aae533.
- M. T. Lam et al. *ApJ*, 819(2):155, Mar. 2016a. doi: 10.3847/0004-637X/819/2/155.
- M. T. Lam et al. *ApJ*, 821(1):66, Apr. 2016b. doi: 10.3847/0004-637X/821/1/66.
- M. T. Lam et al. *ApJ*, 861(1):12, July 2018. doi: 10.3847/1538-4357/aac48d.
- B. Larsen et al. *ApJ*, 972(1):49, Sept. 2024. doi: 10.3847/1538-4357/ad5291.
- P. D. Lasky et al. *Physical Review X*, 6(1):011035, Jan. 2016. doi: 10.1103/PhysRevX.6.011035.
- C. P. Lee et al. *PASA*, 42:e117, Sept. 2025. doi: 10.1017/pasa.2025.10081.
- K. J. Lee. In L. Qain and D. Li, editors, *Frontiers in Radio Astronomy and FAST Early Sciences Symposium 2015*, volume 502 of *Astronomical Society of the Pacific Conference Series*, page 19, Feb. 2016.
- K. J. Lee et al. *MNRAS*, 414(4):3251–3264, July 2011. doi: 10.1111/j.1365-2966.2011.18622.x.
- K. J. Lee et al. *MNRAS*, 423(3):2642–2655, July 2012. doi: 10.1111/j.1365-2966.2012.21070.x.
- K. J. Lee et al. *MNRAS*, 441(4):2831–2844, July 2014. doi: 10.1093/mnras/stu664.
- V. S. H. Lee, A. Mitridate, T. Trickle, and K. M. Zurek. *JHEP*, 06:028, 2021. doi: 10.1007/JHEP06(2021)028.
- L. Lentati et al. *MNRAS*, 437(3):3004–3023, Jan. 2014. doi: 10.1093/mnras/stt2122.
- L. Lentati et al. *MNRAS*, 466(3):3706–3727, Apr. 2017. doi: 10.1093/mnras/stw3359.
- X. Li et al. *arXiv e-prints*, art. arXiv:2506.04871, June 2025. doi: 10.48550/arXiv.2506.04871.
- LIGO Scientific Collaboration et al. *Classical and Quantum Gravity*, 32(7):074001, Apr. 2015. doi: 10.1088/0264-9381/32/7/074001.

- LIGO Scientific Collaboration et al. *arXiv e-prints*, art. arXiv:2508.18080, Aug. 2025. doi: 10.48550/arXiv.2508.18080.
- A. D. Linde. *Physics Letters B*, 108(6):389–393, Feb. 1982. doi: 10.1016/0370-2693(82)91219-9.
- K. Liu et al. *MNRAS*, 417:2916–2926, Sept. 2011. doi: 10.1111/j.1365-2966.2011.19452.x.
- K. Liu et al. *MNRAS*, 420:361–368, Feb. 2012. doi: 10.1111/j.1365-2966.2011.20041.x.
- K. Liu et al. *MNRAS*, 443(4):3752–3760, Oct. 2014. doi: 10.1093/mnras/stu1420.
- K. Liu et al. *MNRAS*, 449:1158–1169, May 2015. doi: 10.1093/mnras/stv397.
- K. Liu et al. *MNRAS*, 463(3):3239–3248, Dec. 2016. doi: 10.1093/mnras/stw2223.
- K. Liu et al. *MNRAS*, 513(3):4037–4044, July 2022. doi: 10.1093/mnras/stac1082.
- K. Liu et al. *MNRAS*, 536(3):2603–2617, Jan. 2025. doi: 10.1093/mnras/stae2727.
- L. Liu, Y.-F. Cai, and M.-Z. Wang. *Physical Review D*, 108(6):063530, 2023. doi: 10.1103/PhysRevD.108.063530.
- T. Liu and S. J. Vigeland. *ApJ*, 921(2):178, Nov. 2021. doi: 10.3847/1538-4357/ac1da9.
- T. Liu, G. Smoot, and Y. Zhao. *Phys. Rev. D*, 101(6):063012, 2020. doi: 10.1103/PhysRevD.101.063012.
- T. Liu, X. Lou, and J. Ren. *Phys. Rev. L.*, 130(12):121401, Mar. 2023. doi: 10.1103/PhysRevLett.130.121401.
- L. Lorenz, C. Ringeval, and M. Sakellariadou. *JCAP*, 10:003, 2010. doi: 10.1088/1475-7516/2010/10/003.
- D. R. Lorimer and M. Kramer. *Handbook of Pulsar Astronomy*. Cambridge University Press, 2004.
- M. E. Lower et al. *MNRAS*, 538(4):3104–3129, Apr. 2025. doi: 10.1093/mnras/staf427.
- J. Luo et al. *ApJ*, 911(1):45, Apr. 2021. doi: 10.3847/1538-4357/abe62f.
- J. Luo et al. *Classical and Quantum Gravity*, 42(17):173001, Sept. 2025. doi: 10.1088/1361-6382/adda8a.
- C. S. Machado, W. Ratzinger, P. Schwaller, and B. A. Stefanek. *JHEP*, 01:053, 2019. doi: 10.1007/JHEP01(2019)053.
- D. R. Madison et al. *ApJ*, 872(2):150, Feb. 2019. doi: 10.3847/1538-4357/ab01fd.
- R. N. Manchester et al. *PASA*, 30:e017, Jan. 2013. doi: 10.1017/pasa.2012.017.
- R. F. Mandow et al. *PASA*, 42:e142, Oct. 2025. doi: 10.1017/pasa.2025.10099.
- M. T. Miles et al. *MNRAS*, 510(4):5908–5915, Mar. 2022. doi: 10.1093/mnras/stab3549.
- M. T. Miles et al. *MNRAS*, 519(3):3976–3991, Mar. 2023. doi: 10.1093/mnras/stac3644.
- M. T. Miles et al. *MNRAS*, 536(2):1467–1488, Jan. 2025a. doi: 10.1093/mnras/stae2572.

- M. T. Miles et al. *MNRAS*, 536(2):1489–1500, Jan. 2025b. doi: 10.1093/mnras/stae2571.
- M. Milosavljević and D. Merritt. In J. M. Centrella, editor, *The Astrophysics of Gravitational Wave Sources*, volume 686 of *American Institute of Physics Conference Series*, pages 201–210, Oct. 2003. doi: 10.1063/1.1629432.
- C. M. F. Mingarelli et al. *Phys. Rev. L.*, 109(8):081104, Aug. 2012. doi: 10.1103/PhysRevLett.109.081104.
- C. M. F. Mingarelli, T. Sidery, I. Mandel, and A. Vecchio. *Phys. Rev. D*, 88(6):062005, Sept. 2013. doi: 10.1103/PhysRevD.88.062005.
- C. M. F. Mingarelli et al. *Nature Astronomy*, 9:183–184, Feb. 2025. doi: 10.1038/s41550-025-02482-1.
- A. Moran et al. *ApJ*, 954(1):89, Sept. 2023. doi: 10.3847/1538-4357/acec75.
- B. E. Moreschi et al. *arXiv e-prints*, art. arXiv:2506.14882, June 2025. doi: 10.48550/arXiv.2506.14882.
- I. S. Morrison et al. *PASA*, 40:e019, Apr. 2023. doi: 10.1017/pasa.2023.15.
- NANOGrav Collaboration et al. *ApJ*, 813(1):65, Nov. 2015. doi: 10.1088/0004-637X/813/1/65.
- R. S. Nathan et al. *MNRAS*, 523(3):4405–4412, Aug. 2023. doi: 10.1093/mnras/stad1660.
- I. C. Nițu et al. *MNRAS*, 528(2):3304–3319, Feb. 2024. doi: 10.1093/mnras/stae220.
- Y. Nomura, N. L. Rodd, and W. A. Terrano. *Phys. Rev. L.*, 125(25):251801, 2020. doi: 10.1103/PhysRevLett.125.251801.
- S. K. Ocker, J. M. Cordes, and S. Chatterjee. *ApJ*, 897(2):124, July 2020. doi: 10.3847/1538-4357/ab98f9.
- S. K. Ocker et al. *ApJ*, 974(1):10, Oct. 2024a. doi: 10.3847/1538-4357/ad6a51.
- S. K. Ocker et al. *MNRAS*, 527(3):7568–7587, Jan. 2024b. doi: 10.1093/mnras/stad3683.
- S. Osłowski et al. *MNRAS*, 418(2):1258–1271, Dec. 2011. doi: 10.1111/j.1365-2966.2011.19578.x.
- S. Osłowski et al. *MNRAS*, 441:3148–3160, July 2014. doi: 10.1093/mnras/stu804.
- L. Oswald et al. arXiv search: Report number AASKAII/Oswald01, 2026.
- A. K. Paladi et al. *MNRAS*, 527(1):213–231, Jan. 2024. doi: 10.1093/mnras/stad3122.
- R. S. Park, W. M. Folkner, J. G. Williams, and D. H. Boggs. *AJ*, 161(3):105, Mar. 2021. doi: 10.3847/1538-3881/abd414.
- A. Parthasarathy et al. *MNRAS*, 502(1):407–422, Mar. 2021. doi: 10.1093/mnras/stab037.
- T. T. Pennucci, P. B. Demorest, and S. M. Ransom. *ApJ*, 790(2):93, Aug. 2014. doi: 10.1088/0004-637X/790/2/93.
- B. B. P. Perera et al. *MNRAS*, 490(4):4666–4687, Dec. 2019. doi: 10.1093/mnras/stz2857.

- P. C. Peters and J. Mathews. *Physical Review*, 131(1):435–440, July 1963. doi: 10.1103/PhysRev.131.435.
- E. S. Phinney. *arXiv e-prints*, art. astro-ph/0108028, Aug. 2001. doi: 10.48550/arXiv.astro-ph/0108028.
- Planck Collaboration et al. *A&A*, 641:A1, Sept. 2020. doi: 10.1051/0004-6361/201833880.
- N. Pol, S. R. Taylor, and J. D. Romano. *ApJ*, 940(2):173, Dec. 2022. doi: 10.3847/1538-4357/ac9836.
- N. K. Porayko and K. A. Postnov. *Phys. Rev. D*, 90(6):062008, 2014. doi: 10.1103/PhysRevD.90.062008.
- N. K. Porayko et al. *MNRAS*, 483(3):4100–4113, Mar. 2019. doi: 10.1093/mnras/sty3324.
- N. K. Porayko et al. *Journal of Geodesy*, 97(12):116, Dec. 2023. doi: 10.1007/s00190-023-01806-1.
- N. K. Porayko et al. *Phys. Rev. D*, 111(6):062005, Mar. 2025. doi: 10.1103/PhysRevD.111.062005.
- N. K. Porayko et al. *Phys. Rev. D*, 98(10):102002, 2018. doi: 10.1103/PhysRevD.98.102002.
- M. S. Pshirkov, D. Baskaran, and K. A. Postnov. *MNRAS*, 402(1):417–423, Feb. 2010. doi: 10.1111/j.1365-2966.2009.15887.x.
- M. Punturo et al. *Classical and Quantum Gravity*, 27(19):194002, Oct. 2010. doi: 10.1088/0264-9381/27/19/194002.
- H. Quelquejay Leclere et al. *Phys. Rev. D*, 108(12):123527, 2023. doi: 10.1103/PhysRevD.108.123527.
- M. Rajagopal and R. W. Romani. *ApJ*, 446:543, June 1995. doi: 10.1086/175813.
- P. Rana et al. *PASA*, 42:e108, July 2025. doi: 10.1017/pasa.2025.10066.
- V. Ravi et al. *MNRAS*, 442(1):56–68, July 2014. doi: 10.1093/mnras/stu779.
- D. J. Reardon et al. *ApJL*, 951(1):L7, July 2023a. doi: 10.3847/2041-8213/acdd03.
- D. J. Reardon et al. *ApJL*, 951(1):L6, July 2023b. doi: 10.3847/2041-8213/acdd02.
- K. J. Rhook and J. S. B. Wyithe. *MNRAS*, 361(4):1145–1152, Aug. 2005. doi: 10.1111/j.1365-2966.2005.08987.x.
- B. J. Rickett. *ARA&A*, 28:561–605, Jan. 1990. doi: 10.1146/annurev.aa.28.090190.003021.
- E. Roebber. *ApJ*, 876(1):55, May 2019. doi: 10.3847/1538-4357/ab100e.
- P. A. Rosado, A. Sesana, and J. Gair. *MNRAS*, 451(3):2417–2433, Aug. 2015. doi: 10.1093/mnras/stv1098.
- W.-H. Ruan, Z.-K. Guo, R.-G. Cai, and Y.-Z. Zhang. *International Journal of Modern Physics A*, 35(17):2050075, June 2020. doi: 10.1142/S0217751X2050075X.

- R. Saito and J. Yokoyama. *Phys. Rev. Lett.*, 102:161101, 2009. doi: 10.1103/PhysRevLett.102.161101. [Erratum: *Phys.Rev.Lett.* 107, 069901 (2011)].
- L. Sampson, N. J. Cornish, and S. T. McWilliams. *Phys. Rev. D*, 91(8):084055, Apr. 2015. doi: 10.1103/PhysRevD.91.084055.
- M. V. Sazhin. *Soviet Ast.*, 22:36–38, Feb. 1978.
- P. Schwaller. *Phys. Rev. Lett.*, 115(18):181101, 2015. doi: 10.1103/PhysRevLett.115.181101.
- F. Semenzato et al. *arXiv e-prints*, art. arXiv:2411.00532, Nov. 2024. doi: 10.48550/arXiv.2411.00532.
- F. Semenzato, N. Bellomo, A. Raccanelli, and C. M. F. Mingarelli. *arXiv e-prints*, art. arXiv:2510.24857, Oct. 2025. doi: 10.48550/arXiv.2510.24857.
- A. Sesana. *Classical and Quantum Gravity*, 30(22):224014, Nov. 2013. doi: 10.1088/0264-9381/30/22/224014.
- A. Sesana and A. Vecchio. *Classical and Quantum Gravity*, 27(8):084016, Apr. 2010. doi: 10.1088/0264-9381/27/8/084016.
- A. Sesana, A. Vecchio, and C. N. Colacino. *MNRAS*, 390(1):192–209, Oct. 2008. doi: 10.1111/j.1365-2966.2008.13682.x.
- A. Sesana, J. Gair, E. Berti, and M. Volonteri. *Phys. Rev. D*, 83(4):044036, Feb. 2011. doi: 10.1103/PhysRevD.83.044036.
- G. Shaifullah, C. Tiburzi, and P. Zucca. *Sol. Phys.*, 295(10):136, Oct. 2020. doi: 10.1007/s11207-020-01705-0.
- R. M. Shannon and J. M. Cordes. *ApJ*, 725(2):1607–1619, Dec. 2010. doi: 10.1088/0004-637X/725/2/1607.
- R. M. Shannon and J. M. Cordes. *MNRAS*, 464(2):2075–2089, Jan. 2017. doi: 10.1093/mnras/stw2449.
- R. M. Shannon et al. *MNRAS*, 443(2):1463–1481, Sept. 2014. doi: 10.1093/mnras/stu1213.
- R. M. Shannon et al. *Science*, 349(6255):1522–1525, Sept. 2015. doi: 10.1126/science.aab1910.
- R. M. Shannon et al. *ApJL*, 828(1):L1, Sept. 2016. doi: 10.3847/2041-8205/828/1/L1.
- E. R. Siegel, M. P. Hertzberg, and J. N. Fry. *MNRAS*, 382:879, 2007. doi: 10.1111/j.1365-2966.2007.12435.x.
- X. Siemens, J. Ellis, F. Jenet, and J. D. Romano. *Classical and Quantum Gravity*, 30(22):224015, Nov. 2013. doi: 10.1088/0264-9381/30/22/224015.
- P. Sikivie. *Phys. Rev. Lett.*, 51:1415–1417, 1983. doi: 10.1103/PhysRevLett.51.1415. [Erratum: *Phys.Rev.Lett.* 52, 695 (1984)].
- J. Singha et al. *MNRAS*, 507(1):L57–L61, Oct. 2021. doi: 10.1093/mnrasl/slab098.

- J. Singha et al. *MNRAS*, 535(1):1184–1192, Nov. 2024. doi: 10.1093/mnras/stae2405.
- C. Smarra et al. *Phys. Rev. Lett.*, 131(17):171001, Oct. 2023. doi: 10.1103/PhysRevLett.131.171001.
- C. Smarra et al. *Phys. Rev. D*, 110(4):043033, Aug. 2024. doi: 10.1103/PhysRevD.110.043033.
- D. A. Smith et al. *ApJ*, 958(2):191, Dec. 2023. doi: 10.3847/1538-4357/acee67.
- R. Spiewak et al. *PASA*, 39:e027, July 2022. doi: 10.1017/pasa.2022.19.
- V. Springel et al. *Nature*, 435(7042):629–636, June 2005. doi: 10.1038/nature03597.
- A. A. Starobinsky. *JETP Lett.*, 30:682–685, 1979.
- N. Steinle et al. *MNRAS*, 525(2):2851–2863, Oct. 2023. doi: 10.1093/mnras/stad2408.
- S. C. Susarla et al. *A&A*, 692:A18, Dec. 2024. doi: 10.1051/0004-6361/202450680.
- A. Susobhanan. *Classical and Quantum Gravity*, 40(15):155014, Aug. 2023. doi: 10.1088/1361-6382/ace234.
- A. Susobhanan, A. Gopakumar, G. Hobbs, and S. R. Taylor. *Phys. Rev. D*, 101(4):043022, Feb. 2020. doi: 10.1103/PhysRevD.101.043022.
- A. Susobhanan et al. *PASA*, 38:e017, Apr. 2021. doi: 10.1017/pasa.2021.12.
- P. Tarafdar et al. *PASA*, 39:e053, Oct. 2022. doi: 10.1017/pasa.2022.46.
- J. H. Taylor and J. M. Weisberg. *ApJ*, 253:908–920, Feb. 1982. doi: 10.1086/159690.
- K. S. Thorne and V. B. Braginskii. *ApJL*, 204:L1–L6, Feb. 1976. doi: 10.1086/182042.
- C. Tiburzi et al. *MNRAS*, 455(4):4339–4350, Feb. 2016. doi: 10.1093/mnras/stv2143.
- C. Tiburzi et al. *MNRAS*, 487(1):394–408, July 2019. doi: 10.1093/mnras/stz1278.
- C. Tiburzi et al. *A&A*, 647:A84, Mar. 2021. doi: 10.1051/0004-6361/202039846.
- C. Tiburzi et al. arXiv search: Report number AASKAII/Tiburzi01, 2026.
- A. Toubiana et al. *A&A*, 700:A135, Aug. 2025. doi: 10.1051/0004-6361/202453027.
- E. Traianou et al. *A&A*, 700:A16, Aug. 2025. doi: 10.1051/0004-6361/202554929.
- M. Tristram et al. *Phys. Rev. D*, 105(8):083524, Apr. 2022. doi: 10.1103/PhysRevD.105.083524.
- R. J. Truant et al. *A&A*, 694:A282, Feb. 2025. doi: 10.1051/0004-6361/202451556.
- T. Vachaspati and A. Vilenkin. *Phys. Rev. D*, 31:3052, 1985. doi: 10.1103/PhysRevD.31.3052.
- M. Vallisneri et al. *ApJ*, 893(2):112, Apr. 2020. doi: 10.3847/1538-4357/ab7b67.
- R. van Haasteren. *ApJSS*, 273(2):23, Aug. 2024. doi: 10.3847/1538-4365/ad530f.
- R. van Haasteren and Y. Levin. *MNRAS*, 401(4):2372–2378, Feb. 2010. doi: 10.1111/j.1365-2966.2009.15885.x.

- W. van Straten. *ApJ*, 642(2):1004–1011, May 2006. doi: 10.1086/501001.
- W. van Straten. *ApJSS*, 204(1):13, Jan. 2013. doi: 10.1088/0067-0049/204/1/13.
- J. P. W. Verbiest and G. M. Shaifullah. *Classical and Quantum Gravity*, 35(13):133001, July 2018. doi: 10.1088/1361-6382/aac412.
- J. P. W. Verbiest et al. *MNRAS*, 458(2):1267–1288, May 2016. doi: 10.1093/mnras/stw347.
- J. P. W. Verbiest et al. *Results in Physics*, 61:107719, June 2024. doi: 10.1016/j.rinp.2024.107719.
- A. Vilenkin. *Phys. Rev. D*, 23:852–857, 1981. doi: 10.1103/PhysRevD.23.852.
- M. Volonteri, F. Haardt, and P. Madau. *ApJ*, 582(2):559–573, Jan. 2003. doi: 10.1086/344675.
- J. B. Wang et al. *MNRAS*, 446(2):1657–1671, Jan. 2015. doi: 10.1093/mnras/stu2137.
- S. Weinberg. *Phys. Rev. D*, 69:023503, 2004. doi: 10.1103/PhysRevD.69.023503.
- P. Weltevrede, R. T. Edwards, and B. W. Stappers. *A&A*, 445:243–272, Jan. 2006. doi: 10.1051/0004-6361:20053088.
- E. Witten. *Phys. Rev. D*, 30(2):272–285, July 1984. doi: 10.1103/PhysRevD.30.272.
- B. E. Wood et al. *ApJ*, 896(2):99, June 2020. doi: 10.3847/1538-4357/ab93b8.
- Y.-M. Wu et al. *Phys. Rev. D*, 106(8):L081101, 2022. doi: 10.1103/PhysRevD.106.L081101.
- Z. Wu et al. *A&A*, 663:A116, July 2022. doi: 10.1051/0004-6361/202142980.
- Z. Wu et al. *MNRAS*, 520(4):5536–5543, Apr. 2023. doi: 10.1093/mnras/stad429.
- J. S. B. Wyithe and A. Loeb. *ApJ*, 590(2):691–706, June 2003. doi: 10.1086/375187.
- Z.-Q. Xia et al. *Phys. Rev. D*, 107(12):L121302, 2023. doi: 10.1103/PhysRevD.107.L121302.
- C. Xin, C. M. F. Mingarelli, and J. S. Hazboun. *ApJ*, 915(2):97, July 2021. doi: 10.3847/1538-4357/ac01c5.
- H. Xu et al. *Research in Astronomy and Astrophysics*, 23(7):075024, July 2023. doi: 10.1088/1674-4527/acdfa5.
- X. Xue et al. *Phys. Rev. L.*, 136(1):011001, Jan. 2026. doi: 10.1103/mptv-3x6g.
- X. Xue et al. *Phys. Rev. Lett.*, 127(25):251303, 2021. doi: 10.1103/PhysRevLett.127.251303.
- X. Xue et al. *Phys. Rev. Res.*, 4(1):L012022, 2022. doi: 10.1103/PhysRevResearch.4.L012022.
- N. Yonemaru et al. *MNRAS*, 501(1):701–712, 2021. doi: 10.1093/mnras/staa3721.
- X. P. You et al. *MNRAS*, 378(2):493–506, June 2007. doi: 10.1111/j.1365-2966.2007.11617.x.
- X.-X. Zeng et al. *arXiv e-prints*, art. arXiv:2504.11275, Apr. 2025. doi: 10.48550/arXiv.2504.11275.
- S.-Y. Zhao et al. *ApJ*, 992(2):181, Oct. 2025. doi: 10.3847/1538-4357/ae0719.

W. Zhao, Y. Zhang, X.-P. You, and Z.-H. Zhu. *Phys. Rev. D*, 87(12):124012, 2013. doi: 10.1103/PhysRevD.87.124012.

Q. Zheng et al. *Phys. Rev. D*, 113(2):023037, Jan. 2026. doi: 10.1103/dkjh-kfqq.

A. Zic et al. *MNRAS*, 516(1):410–420, Oct. 2022. doi: 10.1093/mnras/stac2100.

A. Zic et al. *PASA*, 40:e049, Dec. 2023. doi: 10.1017/pasa.2023.36.